an indirect effect of GM via good vertigo control as discussed in the above paragraph. Premedication audiometry could not predict the hearing outcome of the GM treatment (Table 2).

Plasma AVP level, as a marker of stress (9), was lower in the hearing improvement group than in the hearing loss/no changes group before GM injections (Table 2). It further decreased after intratympanic GM only in Group II, although it tended to increase in Group I (Fig. 4). The second observation is in line with a recent study that reported a decrease of plasma AVP after endolymphatic sac drainage surgery, especially in patients with good vertigo control (19). The mechanisms effective in the control of vertigo by intratympanic GM injections and endolymphatic sac drainage surgery are different, but the decrease of plasma AVP after both treatments seems to be induced by a factor common to these two treatments, namely the reduction of stress after good vertigo control. It is suggested that patients' stress level may be related to the hearing response to GM treatment, and good posttherapy vertigo control would reduce the level of stress.

In conclusion, premedication hearing level (stage of Ménière's disease) and an increase of CP% with induction of post-HSN (damage of the vestibular periphery) are the key factors for the control of vertigo after GM treatment. Hearing outcome is affected by the control of vertigo after GM injections and by the stress level before treatment.

Acknowledgment: We thank Dr. Kalubi Bukasa for his comments on the manuscript.

REFERENCES

1. Gates GA. Ménière's disease: medical therapy. In: Harris JP, ed. *Ménière's Disease*. The Hague: Kugler Publications, 1999:329–40.
2. Jackson CG, Dickins JR, McMenomey SO, et al. Endolymphatic system shunting: a long-term profile of the Denver Inner Ear Shunt. *Am J Otolaryngol* 1996;17:85–8.
3. Blakley BW. Update on intratympanic gentamicin for Ménière's disease. *Laryngoscope* 2000;110:236–40.
4. Kaplan DM, Nedzelski JM, Chen JM, Shipp DB. Intratympanic gentamicin for the treatment of unilateral Ménière's disease. *Laryngoscope* 2000;110:1298–305.
5. Harner SG, Driscoll CL, Facer GW, Beatty CW, McDonald TJ. Long-term follow-up of transtympanic gentamicin for Ménière's syndrome. *Otol Neurotol* 2001;22:210–4.
6. Chia SH, Gamst AC, Anderson JP, Harris JP. Intratympanic gentamicin therapy for Ménière's disease: a meta-analysis. *Otol Neurotol* 2004;25:544–52.
7. Cohen-Kerem R, Kisilevsky V, Einarson TR, Kozer E, Koren G, Rutka JA. Intratympanic gentamicin for Ménière's disease: a meta-analysis. *Laryngoscope* 2004;114:2085–91.
8. Light JP, Silverstein H. Transtympanic perfusion: indications and limitations. *Curr Opin Otolaryngol Head Neck Surg* 2004;12: 378–83.
9. Charmandari E, Tsigos C, Chrousos G. Endocrinology of the stress response. *Annu Rev Physiol* 2005;67:259–84.
10. Committee on Hearing and Equilibrium. Committee on hearing and equilibrium guidelines for the diagnosis and evaluation of therapy in Ménière's disease. *Otolaryngol Head Neck Surg* 1995; 113:181–5.
11. Kaasinen S, Pyykko I, Ishizaki H, Aalto H. Intratympanic gentamicin in Ménière's disease. *Acta Otolaryngol* 1998;118:294–8.
12. Perez N, Martin E, Garcia-Tapia R. Intratympanic gentamicin for intractable Ménière's disease. *Laryngoscope* 2003;113:456–64.
13. Light JP, Silverstein H, Jackson LE. Gentamicin perfusion vestibular response and hearing loss. *Otol Neurotol* 2003;24:294–8.
14. de Waele C, Meguenni R, Freyss G, et al. Intratympanic gentamicin injections for Ménière disease: vestibular hair cell impairment and regeneration. *Neurology* 2002;59:1442–4.
15. Pender DJ. Gentamicin tympanoclysis: effects on the vestibular secretory cells. *Am J Otolaryngol* 1985;6:358–67.
16. Adamonis J, Stanton SG, Cashman MZ, Mattan K, Nedzelski JM, Chen JM. Electrocochleography and gentamicin therapy for Ménière's disease: a preliminary report. *Am J Otolaryngol* 2000; 21:534–42.
17. Cureoglu S, Schachern PA, Paparella MM. Effect of parenteral aminoglycoside administration on dark cells in the crista ampullaris. *Arch Otolaryngol Head Neck Surg* 2003;129:626–8.
18. Wu IC, Minor LB. Long-term hearing outcome in patients receiving intratympanic gentamicin for Ménière's disease. *Laryngoscope* 2003;113:815–20.
19. Horii A, Kitahara T, Uno A, et al. Vestibular function and vasopressin. *Acta Otolaryngol Suppl* 2004;553:50–3.

BRAIN RESEARCH 1138 (2007) 129–135

available at www.sciencedirect.com

ScienceDirect

www.elsevier.com/locate/brainres

BRAIN RESEARCH

Research Report

Unilateral vestibular deafferentation-induced changes in calcium signaling-related molecules in the rat vestibular nuclear complex

Chisako Masumura, Arata Horii, Kenji Mitani, Tadashi Kitahara, Atsuhiko Uno, Takeshi Kubo*

Department of Otolaryngology, Osaka University School of Medicine, 2-2 Yamadaoka, Suita, Osaka 565-0871, Japan

ARTICLE INFO

Article history:
Accepted 27 December 2006
Available online 30 December 2006

Keywords:
Vestibular compensation
Calcium channel
Calcineurin
Plasma membrane Ca^{2+} ATPase (PMCA)

ABSTRACT

Inquiries into the neurochemical mechanisms of vestibular compensation, a model of lesion-induced neuronal plasticity, reveal the involvement of both voltage-gated Ca^{2+} channels (VGCC) and intracellular Ca^{2+} signaling. Indeed, our previous microarray analysis showed an up-regulation of some calcium signaling-related genes such as the α2 subunit of L-type calcium channels, calcineurin, and plasma membrane Ca^{2+} ATPase 1 (PMCA1) in the ipsilateral vestibular nuclear complex (VNC) following unilateral vestibular deafferentation (UVD). To further elucidate the role of calcium signaling-related molecules in vestibular compensation, we used a quantitative real-time polymerase chain reaction (PCR) method to confirm the microarray results and investigated changes in expression of these molecules at various stages of compensation (6 h to 2 weeks after UVD). We also investigated the changes in gene expression during Bechterew's phenomenon and the effects of a calcineurin inhibitor on vestibular compensation. Real-time PCR showed that genes for the α2 subunit of VGCC, PMCA2, and calcineurin were transiently up-regulated 6 h after UVD in ipsilateral VNC. A subsequent UVD, which induced Bechterew's phenomenon, reproduced a complete mirror image of the changes in gene expressions of PMCA2 and calcineurin seen in the initial UVD, while the α2 subunit of VGCC gene had a trend to increase in VNC ipsilateral to the second lesion. Pre-treatment by FK506, a calcineurin inhibitor, decelerated the vestibular compensation in a dose-dependent manner. Although it is still uncertain whether these changes in gene expression are causally related to the molecular mechanisms of vestibular compensation, this observation suggests that after increasing the Ca^{2+} influx into the ipsilateral VNC neurons via up-regulated VGCC, calcineurin may be involved in their synaptic plasticity. Conversely, an up-regulation of PMCA2, a brain-specific Ca^{2+} pump, would increase an efflux of Ca^{2+} from those neurons and perhaps prevent cell damage following UVD.

* *Corresponding author.* Fax: +81 6 6879 3959.
E-mail address: ahorii@ent.med.osaka-u.ac.jp (A. Horii).

Abbreviations: ANOVA, analysis of variance; CaMK II, Ca^{2+}/calmodulin-dependent protein kinase II; CT, cycle of threshold; LTD, long-term depression; LTP, long-term potentiation; MVN, medial vestibular nucleus; NMDA, *N*-methyl-D-aspartate; PCR, polymerase chain reaction; PKC, protein kinase C; PMCA, plasma membrane Ca^{2+} ATPase; UVD, unilateral vestibular deafferentation; VGCC, voltage gated calcium channel; VNC, vestibular nuclear complex

0006-8993/$ – see front matter © 2007 Elsevier B.V. All rights reserved.
doi:10.1016/j.brainres.2006.12.072

1. Introduction

Following unilateral vestibular deafferentation (UVD), many of the oculomotor and postural symptoms that persist in the absence of head movement, such as spontaneous ocular nystagmus and head tilt (i.e., 'static symptoms'), gradually abate over time in a process known as 'vestibular compensation' (Smith and Curthoys, 1989; Dieringer, 1995; Curthoys and Halmagyi, 1995). After compensation, a lesion to the remaining labyrinth triggers a new postural and oculomotor syndrome, which is similar to the one induced by the initial lesion but oriented in the opposite direction. This is known as Bechterew's phenomenon.

Regarding the neurochemical mechanisms of vestibular compensation, several lines of evidence suggest an involvement of voltage-gated Ca^{2+} channels (VGCC) and intracellular Ca^{2+} signaling. It has been reported that in normal conditions medial vestibular nucleus (MVN) neurons exhibit both of high- and low-threshold Ca^{2+} currents, possibly involving L-, N-, and T-types VGCC, respectively (Serafin et al., 1991; Him and Dutia, 2001). In addition, a number of neurons in the ipsilateral MVN exhibiting low-threshold Ca^{2+} currents and capable of generating pacemaker activity, increased after UVD (Ris et al., 2003). Pharmacological studies demonstrated an acceleration of static symptom compensation in guinea pigs (Tolu et al., 1988; Darlington and Smith, 1992) and frogs (Leinhos and Flohr, 1992) after administration of VGCC antagonists such as flunarizine or verapamil, though a later report contradicted that result (Gilchrist et al., 1993). These studies suggest an involvement of Ca^{2+} channels in vestibular compensation.

Ca^{2+} is also known to play an important role as an intracellular second messenger as demonstrated by several studies suggesting involvement of Ca^{2+}-dependent phosphorylation in neuronal plasticity of the CNS (Xia and Storm, 2005). In normal conditions, immunohistochemistry and in situ hybridization studies showed a distribution of both mRNAs and protein content of protein kinase C (PKC) isoforms in the VNC (Tanaka and Saito, 1992) and Ca^{2+}/calmodulin-dependent protein kinase II (CaMK II) in the brainstem (Ochiishi et al., 1998). Also, a number of studies have investigated the effects of inhibitors of these kinases on vestibular compensation. Accordingly, selective PKC inhibitors increased the frequency of spontaneous nystagmus at an early stage after UVD (Balaban et al., 1999; Sansom et al., 2000). Moreover, an in vitro phosphorylation assay showed that vestibular compensation is accompanied by specific changes in the phosphorylation of several major PKC substrates in the VNC (Sansom et al., 1997; Kerr et al., 2000). All these observations suggest an important role for Ca^{2+} channels and Ca^{2+}-dependent intracellular signaling pathways in vestibular compensation.

In a previous study, we used a microarray analysis to examine genes showing asymmetrical expressions between bilateral vestibular nuclear complex (VNC) 6 h after UVD (Horii et al., 2004). This study revealed an up-regulation of some calcium signaling-related genes such as the α2 subunit of L-type calcium channels, calcineurin, and plasma membrane Ca^{2+} ATPase 1 (PMCA1) in the ipsilateral VNC. The α2 subunit of calcium channels appears to be one of the constituents of the L-type VGCC, which may be involved in Ca^{2+} influx following UVD in the vestibular nucleus neurons. Calcineurin is a Ca^{2+}/calmodulin-dependent protein phosphatase, which is suggested to play a role in neuronal plasticity in ocular dominance plasticity model (Yang et al., 2005), whereas PMCA1 has been demonstrated to act as a Ca^{2+} pump which is important for Ca^{2+} efflux when intracellular Ca^{2+} concentration increases (Carafoli, 1994). Taken together with the microarray results and previous reports indicating an important role for Ca^{2+} and Ca^{2+}-dependent signaling in vestibular compensation, we focused in this study on the α2 subunit of the Ca^{2+} channel, calcineurin, and PMCA2, another isoform of PMCA specific to brain tissue. The aims of this study were four-fold: first, to confirm our microarray results using a quantitative real-time PCR, second to further investigate changes in the expression of these molecules at the various stages of compensation (6 h, 24 h, 50 h, and 2 weeks after UVD), third to further confirm the changes in gene expression during Bechterew's phenomenon, and finally to investigate the effects of calcineurin inhibitors on vestibular compensation by measuring the number of spontaneous nystagmus beats following UVD.

2. Results

2.1. *Real-time PCR*

Fig. 1 shows the changes in mRNA expression of the α2 subunit of VGCC (Fig. 1A), PMCA2 (Fig. 1B), and calcineurin (Fig. 1C) following UVD. The gene expressions of the α2 subunit of VGCC (Fig. 1A, $p<0.05$) and that of calcineurin (Fig. 1C, $p<0.05$) were significantly higher in the ipsilateral VNC as compared to those of the contralateral side at 6 h post-UVD. This right–left difference disappeared at 24 h and there were no changes until 2 weeks after UVD. The gene expression of PMCA2 in the ipsilateral VNC at 6 h post-UVD was significantly higher than that from 24 h to 2 weeks post-UVD (Fig. 1B, $p<0.01$). Although the right–left difference in the gene expression of PMCA2 at 6 h post-UVD did not reach statistically significant levels ($p=0.0608$), it gradually decreased with the time (Fig. 1B).

Fig. 2 shows the gene expression of the α2 subunit of VGCC (Fig. 2A), PMCA2 (Fig. 2B), and calcineurin (Fig. 2C) during Bechterew's phenomenon. Second UVD for left ear performed 2 weeks after the first UVD induced Bechterew's phenomenon for all animals: at the time of the second UVD, all static symptoms recovered following a right UVD and the second UVD to the left side induced a spontaneous nystagmus to the right side and head tilt to the left side. Six hours following the second UVD, the gene expression of PMCA2 and calcineurin was significantly higher in left VNC than right VNC ($p<0.05$), while that of the α2 subunit of VGCC had a trend, but without statistically significance, to increase in the left VNC.

2.2. *Effects of FK506 on UVD-induced spontaneous nystagmus*

As shown in Fig. 3, the number of spontaneous nystagmus beats in FK506 treated groups (>5 mg/kg) was significantly higher compared to those of the control group. In FK506 at

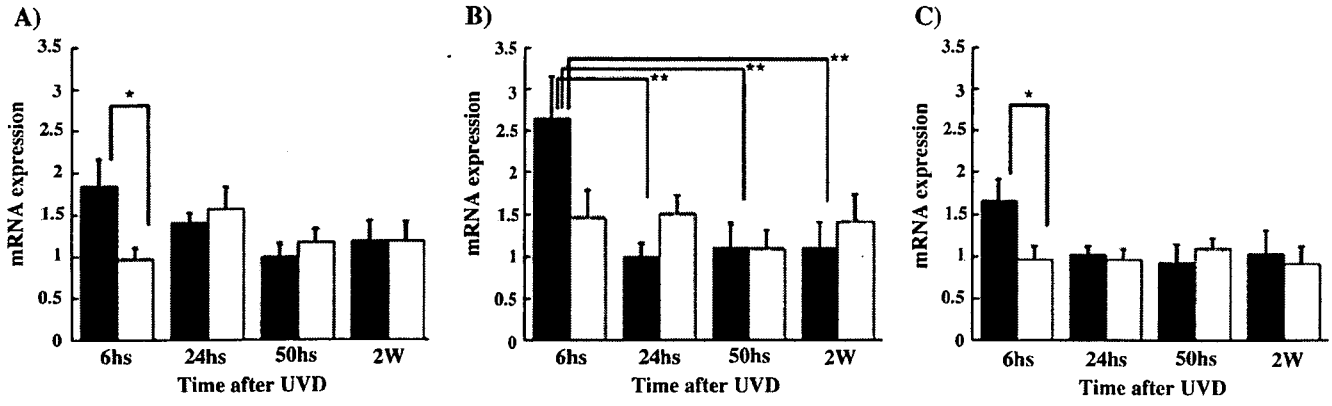

Fig. 1 – Changes in gene expression of Ca^{2+}-related molecules in the VNC following UVD. (A) α2 subunit of VGCC; (B) PMCA2; (C) calcineurin; closed column, ipsilateral (right) VNC; open column, contralateral (left) VNC. *$p<0.05$, **$p<0.01$. Gene expressions of the α2 subunit of VGCC (A, $p<0.05$) and calcineurin (C, $p<0.05$) in the ipsilateral VNC (closed column) were significantly higher compared to those from the contralateral VNC (open column) at 6 h post-UVD. Gene expression of PMCA2 in the ipsilateral VNC at 6 h post-UVD was significantly higher than those at 24 h to 2 weeks post-UVD (B, $p<0.01$).

10 mg/kg group, the difference was significant 18–48 h post-UVD ($p<0.01$). In 5 mg/kg group, it was significant 24–48 h post-UVD ($p<0.01$). Among FK506-treated animals, the groups treated with 5 or 10 mg/kg showed a significantly higher number of spontaneous nystagmus beats at 12 h and 18 h post-UVD compared to those of the 1 mg/kg group ($p<0.01$). It was demonstrated that systemic administration of FK506 30 min prior to UVD significantly increased the number of spontaneous nystagmus beats in a dose-dependent manner.

3. Discussion

The present real-time quantitative PCR studies demonstrated that gene expression of the α2 subunit of VGCC and calcineurin was up-regulated in the ipsilateral VNC 6 h post-UVD, which confirms our previous microarray results (Horii et al., 2004). PMCA2, a brain-specific isoform of PMCA, was also up-regulated in the ipsilateral VNC 6 h post-UVD, while the up-regulation of PMCA1 was demonstrated by the microarray study. Taken together, the up-regulation of these genes 6 h post-UVD in the ipsilateral VNC was demonstrated by two different methods, namely the microarray analysis and real-time PCR, indicating that these changes are convincing.

Following compensation from an initial labyrinthectomy, a lesion to the remaining labyrinth triggers Bechterew's phenomenon. Indeed, a new postural and oculomotor syndrome appears, similar to the one induced by the initial lesion, but oriented in the opposite direction. In the present study, the changes induced in PMCA2 and calcineurin genes by the second lesion were the complete mirror images of those observed after the initial labyrinthectomy, indicating that these changes are strongly related to the lesion of the labyrinth. Gene expression of the α2 subunit of VGCC tended to increase in VNC ipsilateral to the second lesion without statistically significance. The intensity of Bechterew's syndrome reflects the recovering level of spontaneous activity on the initially deafferentated side at the time of the second lesion

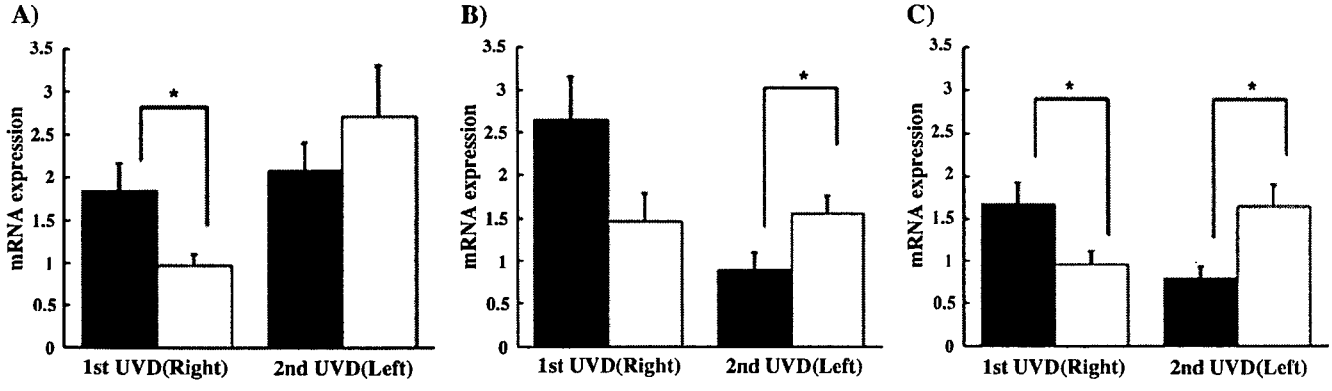

Fig. 2 – Gene expression of Ca^{2+}-related molecules in the VNC during Bechterew's phenomenon. (A), α2 subunit of VGCC; (B), PMCA2; (C), calcineurin; closed column, right VNC; open column, left VNC. *$p<0.05$. Second UVD-induced changes in gene expressions of PMCA2 (B) and calcineurin (C) showed a complete mirror image of those observed after the first UVD. Changes in gene expressions for the α2 subunit of VGCC (A) had a trend, but without statistically significance, to increase in VNC ipsilateral to the second UVD.

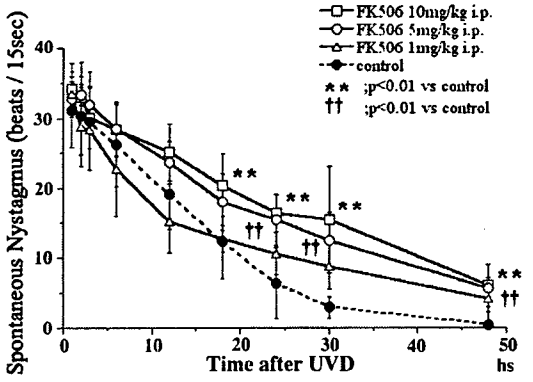

Fig. 3 – Effects of FK506 on UVD-induced spontaneous nystagmus. In the group of animals treated by FK506 at a dose of 10 mg/kg, the number of spontaneous nystagmus was significantly higher 18–48 h post-UVD compared to the control ($p<0.01$). In 5 mg/kg group, it was significant 24–48 h post-UVD ($p<0.01$). Among FK506-treated groups, the 5 or 10 mg/kg group showed a significantly higher number of spontaneous nystagmus beats at 12 and 18 h post-UVD compared to that of 1 mg/kg group ($p<0.01$).

(Vibert et al., 1999). It is suggested that although the behavioral recoveries (i.e., spontaneous nystagmus and head tilt) were seen after the initial UVD, the incomplete recovery of the VNC neurons on the initially deafferentated side may explain the present results for the α2 subunit of VGCC, i.e., just a tendency without significance. Nevertheless, the opposite direction of changes in gene expression during Bechterew's phenomenon indicates that the changes observed were convincing and strongly related to the lesion of the labyrinth.

The expression of these three genes returned to the baseline level 24 h post-UVD and there were no changes until 2 weeks post-UVD, indicating that up-regulation of these genes was just transient in the ipsilateral VNC. Although this study has limitations that it is uncertain whether these changes observed are just a consequence of deafferentation and loss of sensory inputs or causally related to the plasticity mechanisms, we would like to draw the following discussion based on the current and the previous data.

The α2 subunit of VGCC was increased in the ipsilateral VNC following UVD. The up-regulation of VGCC in the ipsilateral VNC fits with the "Ca^{2+} hypothesis" of vestibular compensation (Darlington and Smith, 1996). Accordingly, excessive Ca^{2+} enters into VNC neurons via ligand-activated channels (*N*-methyl-D-aspartate (NMDA) glutamate receptors) and/or VGCC following UVD might interfere with functioning of ipsilateral VNC neurons. The same hypothesis predicts an increase of NMDA receptors and VGCC in the ipsilateral VNC. We suggest that Ca^{2+} influx into the ipsilateral VNC neurons may be increased by the up-regulation of the α2 subunit of VGCC, while a trigger inducing this up-regulation and an increased intracellular Ca^{2+} concentration after UVD should be investigated in future studies.

Intracellular Ca^{2+} concentration is maintained by a balance of the influx and efflux of both the extra- and intracellular Ca^{2+} storage. In mice with a point mutation in PMCA2, a brain-specific Ca^{2+} pump, Ca^{2+} influx was reduced in cerebellar neurons via down-regulation of VGCC (Ueno et al., 2002). By contrast, it is reported that neuronal differentiation-induced up-regulation of Ca^{2+} channels increased the expression of functional and protein levels of PMCA2 and thus paralleling the amplification of Ca^{2+} influx and efflux pathways that are active during differentiation to maintain intracellular Ca^{2+} concentration (Usachev et al., 2001). Therefore, we assume that an increase in PMCA2 expression in the ipsilateral VNC 6 h post-UVD was a downstream effect of the up-regulation of VGCC and a possible increase in intracellular Ca^{2+} concentration. These mechanisms may act to keep a constant intracellular Ca^{2+} concentration to prevent cell death in the ipsilateral VNC after UVD. Indeed, just an impaired function but not a massive cell death was noted after deafferentation in the VNC, and once the VNC was lesioned, no compensation occurred (Smith and Curthoys, 1989).

The induction of synaptic plasticity is believed to depend on the balance between opposing regulatory factors, such as protein kinases and protein phosphatases (Lisman, 1989). Although vestibular compensation is one of many models of neuronal plasticity, molecular mechanisms underlying each model may be different between models. As summarized in the introduction section, the role of protein kinases in the vestibular compensation has been well documented. However, there has been no study focusing on the other regulatory factor, protein phosphatase, in the VNC. Calcineurin, the only Ca^{2+}/calmodulin-activated protein phosphatase in the brain, has been recently suggested to be involved in a neuronal plasticity such as an ocular dominance plasticity (Yang et al., 2005). Several forms of synaptic plasticity including long-term potentiation (LTP) and long-term depression (LTD) are initiated by increases in intracellular Ca^{2+} through NMDA receptors or VGCC followed by coordinated regulation of an ensemble of enzymes, including Ca^{2+}/calmodulin-dependent protein kinase II, adenylyl cyclase 1 and 8, and calcineurin (Xia and Storm, 2005). In the present study, the α2 subunit of VGCC and calcineurin was transiently up-regulated in the ipsilateral VNC following UVD. It can be assumed that increased Ca^{2+} entries and the following activation of calcineurin may occur in the ipsilateral VNC neurons immediately after UVD. In general, protein phosphorylation by kinases facilitates synaptic plasticity and memory function, while dephosphorylation by phosphatases negatively modulates it (Abel et al., 1998; Mansuy, 2003). However, some reports contradict this theory (Beaumont et al., 2001). For example, in cerebellar slices, a recent study demonstrated that serine/threonine phosphatases including calcineurin are involved in the LTP induction (Belmeguenai and Hansel, 2005). Taken together with previous studies using phosphorylation assays (Sansom et al., 1997; Kerr et al., 2000) and kinase inhibitors (Balaban et al., 1999; Sansom et al., 2000), the present results suggest that the synaptic plasticity following deafferentation in the VNC neurons may be modulated by both the protein phosphorylation and dephosphorylation.

To further confirm the role of calcineurin in the development of vestibular compensation, we investigated the effects with pre-treatment of FK506, a calcineurin inhibitor, on vestibular compensation. Regarding the effects of FK506 on the nervous system, it is reported that FK506 not only accelerated the regeneration of injured sciatic nerve (Gold

et al., 1995), but also had neuroprotective effects (Sharkey and Butcher, 1994). The present results showed that injection of FK506 30 min prior to UVD increased the number of UVD-induced spontaneous nystagmus from 18 to 48 h post-UVD in a dose-dependent manner. It is reported that intravenous injection of FK506 at a dose of 5 mg/kg produced the maximum inhibition of calcineurin activity in whole blood 24 h after drug administration (Fukudo et al., 2005). This could account for the delayed effects of FK506 on the number of UVD-induced nystagmus beats in this study. One shot injection of FK506 at a dose of 5–10 mg/kg is relatively high dose compared to those used in previous studies (Gold et al., 1995; Fukudo et al., 2005), however, it is not an extremely high dose. Dose-dependent fashion of the effects of FK506 strongly suggests that a calcineurin inhibitor decelerates vestibular compensation. This is somewhat a surprising finding, because inhibitors of protein kinases also decelerated the vestibular compensation (Balaban et al., 1999; Sansom et al., 2000). Taken together with the up-regulation of the calcineurin gene in the ipsilateral VNC 6 h post-UVD, calcineurin had facilitative effects on synaptic plasticity following deafferentation of the vestibular nerve. Taken together with previous reports demonstrating that protein kinase inhibitors decelerated the vestibular compensation (Balaban et al., 1999; Sansom et al., 2000), it is suggested that both phosphorylation and dephosphorylation need to occur in order for normal compensation to occur.

In conclusion, transient up-regulation of the α2 subunit of VGCC, PMCA2, and calcineurin genes in the ipsilateral VNC was demonstrated 6 h post-UVD. During Bechterew's phenomenon, changes in gene expressions of PMCA2 and calcineurin genes detected following the second UVD were the complete mirror images with the initial UVD, indicating that up-regulation of PMCA2 and calcineurin genes by UVD was strongly related to the lesion of the labyrinth. Pretreatment of FK506, a calcineurin inhibitor, decelerated the vestibular compensation. It is suggested that an increased expression of the α2 subunit of VGCC may be involved in Ca^{2+} entries into neurons after UVD, and it would raise a Ca^{2+} concentration in neurons by which calcineurin would be activated. Cacineurin would then induce vestibular compensation by acting on the phosphorylation state of target proteins. An up-regulation of PMCA2, a brain-specific Ca^{2+} pump, would increase an efflux of Ca^{2+} and perhaps prevent cell damage following UVD.

4. Experimental procedures

4.1. *Unilateral vestibular deafferentation and Bechterew's phenomenon*

All animal experiments were approved by the Animal Care Committee of Osaka University School of Medicine. Seven week-old male Wistar strain rats weighing approximately 140–160 g were used. Weight of animals at the time of sacrifice in the chronic experiments to examine Bechterew's phenomenon varied from 140 g to 190 g. All surgeries were performed between 10:00 and 15:00 to minimize the circadian effects on gene expression. Twenty-nine animals were anesthetized with pentobarbital (40 mg/kg, i.p.) and underwent a right UVD, using a retro-auricular approach. Local anesthesia with 1% lidocaine was also used in the wound margin. After removal of the tympanic membrane, malleus, and incus, the vestibule just above the ampullae of the horizontal and anterior semicircular canals was drilled out. After aspiration of labyrinthine fluids and the membraneous labyrinth from the drilled vestibule and the ventral portion of the oval window, the labyrinth was rinsed with 0.1 ml of absolute ethanol, and perfused through the ventral portion of the oval window and the drilled vestibule. Our previous histological studies showed that this procedure completely destroyed the labyrinth and that the lesion did not extend to adjacent regions such as the ganglion cells (Horii et al., 2004). For the sham operation group, 27 animals had their right retro auricular skin incised in the same way as for the UVD with preservation of the tympanic membrane, malleus, and incus. Six, 24, 50 h, and 2 weeks following the right UVD or sham operation, the animals were deeply anesthetized with an over-dose of pentobarbital before their brains were removed. Six hours-post-UVD corresponds to time point that the animals show vigorous vestibular symptoms, while 50 h and 2 weeks correspond to substantial and complete compensation of the vestibular symptoms, respectively. The number of animals used for post-UVD experiments was: 9 for 6 h, 7 for 24 h, 6 for 50 h, and 7 for 2 weeks. For post-sham operation experiments, the distribution of animals was as follows: 6 for 6 h, 7 for 24 h, 6 for 50, and 8 for 2 weeks.

In addition, eight animals were used to investigate the effects of a second vestibular deafferentation on the changes in gene expressions in the VNC in compensated animals following UVD and those showing Bechterew's phenomenon. Two weeks after a right UVD, the animals underwent a contralateral (left) UVD by the same method as the right side. Accordingly, all animals showed Bechterew's phenomenon: at the time of the second UVD, all static symptoms that had recovered following a right UVD were re-activated following the second UVD, with animals showing a spontaneous nystagmus beating to the right side and a head tilt to the left side (data not shown). Six hours following the second UVD, animals were sacrificed and the brains were removed.

4.2. *Dissection of tissues and RNA extraction*

Horizontal brainstem slices including the VNC (1.5 mm thickness) were taken just caudal from the abducens nucleus. Then, the bilateral VNCs were dissected separately under microscopic guidance using a sharp blade. The dissections were performed symmetrically using the detailed procedures we have described previously (Horii et al., 2001, 2002). All of these procedures were performed on a chilled plate in order to prevent possible RNA degradation. Total RNA was extracted using an RNeasy Mini Kit (Qiagen, Germany) according to the manufacturer's instructions. RNA was not pooled but each RNA from one sample was forwarded to real-time PCR separately. The mean and range of final RNA concentration from one sample was 30.8 μg/ml (23.0–36.9), indicating that there was less variability of dissecting the brain tissue.

4.3. *Real-time PCR*

The detailed procedures for the real-time quantitative PCR method have been published previously (Horii et al., 2001, 2002, 2003, 2004). Briefly, PCR was carried out with TaqMan Universal PCR Master Mix (Perkin Elmer). Each target molecule was coamplified with primers and the TaqMan probe for GAPDH in the same PCR tube. The final concentration of each oligonucleotide in the PCR reaction was as follows: GAPDH primer, 200 nM; primer for target molecule, 400 nM; TaqMan probe for GAPDH and target molecule, 200 nM each. One microliter of cDNA was forwarded to PCR and the total reaction volume of PCR was 20 μl. Thermal cycling was initiated with incubation at 50 °C for 2 min and 95 °C for 10 min. After this initial step, 40 cycles of PCR were performed. Each PCR cycle consisted of heating at 95 °C for 15 s for melting and 60 °C for 1 min for annealing and extension.

The amplification plots from fluorescent emission data collected during the PCR were constructed using the ABI7900 model software. CT (cycle of threshold) values corresponding to the number of PCR cycles at which the fluorescence emission monitored in real-time exceeded a threshold limit (10 times the standard deviation of the baseline intensity) were measured. The PCR assays for unknown samples were performed simultaneously with standard samples (i.e., cerebellar cortex of untreated animals) and negative control samples (non-reverse transcription samples) in the same plate. The standard cDNA was diluted in 4 steps from 2 to 2^4 times and a standard curve plotting CT values against input quantity was constructed for both GAPDH and the target molecule in every PCR assay. The relative concentration of GAPDH and the target molecule of unknown samples was calculated from this standard curve, and the ratio of the relative concentration of the target molecule to GAPDH (target molecule/GAPDH) of unknown samples was calculated. This ratio represented the relative expression of the target molecule of the unknown sample compared to the standard sample, which had been normalized by GAPDH expression. Possible variability in the initial amount of total RNA in each sample was controlled by this calibration procedure in which the target molecule was co-amplified with an endogenously expressed GAPDH as an internal standard in the same PCR tube. Finally, the ratio (UVD/sham) of gene expression of each target molecule following each period (6 h, 24 h, 50 h, and 2 weeks) was calculated.

Sequences and fluorescent dyes of PCR primers and TaqMan probes specific for the target molecules (α2 subunit of VGCC, calcineurin, PMCA2) and glyceraldehyde-3-phosphate dehydrogenase (GAPDH) were as follows. α2 subunit of VGCC, forward primer 5′-TTCCCTGAACACCGCACATA-3′, reverse primer 5′-CGCTG GTCACTGGGCACTAT-3′, probe 5′-CACTGAGAAC-CACGGGACTGGCAAC-3′; calcineurin, forward primer 5′-CAC-CAAGAGAAGCTCCACCC-3′, reverse primer probe 5′-AGAATG-ACAGGGCTTGGGC-3′, probe 5′-CCATTTATGAGACGCCACC-TACGCTCC-3′; PMCA2, forward primer 5′-CCATCTGTTGG-CTCCCCTT-3′, reverse primer 5′-TCTGCCCTACTGATGTCC-TGC-3′, probe 5′-AGACCCAGCAGCTCCAGGCTTCCT-3′; GAPDH, forward primer 5′-TGCACCACCAACTGCTTAG-3′, reverse primer 5′-GGATGCAGGGATGATGTTC-3′, probe 5′-VIC-CAGAA-GACTGTGGATGGCCCCTC-TAMRA-3′.

4.4. *Effects of FK506 on UVD-induced spontaneous nystagmus*

Thirty-one rats underwent UVD by the same procedure described above under ether anesthesia, which enabled a counting of spontaneous nystagmus beats just after the UVD. Animals were divided into four groups that received an intraperitoneal injection of FK506 either at a dose of 1 mg/kg ($n=9$), 5 mg/kg ($n=7$), 10 mg/kg ($n=7$) or saline (2 ml/kg) as a control ($n=8$) 30 min prior to the UVD. FK506, a calcineurin antagonist used in this study, was a courtesy gift from Astelas Pharmaceutical Co., Ltd. Osaka, Japan. Dose and time of FK506 injection were chosen referring to the previous report on its effect to the rat (Butcher et al., 1997). Each rat was kept individually for 48 h and the number of spontaneous nystagmus beats was counted for 15 s at 1, 2, 3, 6, 12, 18, 24, 30, and 48 h after UVD using a video camera (FV200, Canon Inc., Tokyo, Japan). The average score of the three measurements of nystagmus beats was statistically evaluated.

4.5. *Statistics*

The statistical significance of differences at each time point (mRNA expression of target molecules and the number of spontaneous nystagmus beats) was analyzed by one-way factorial ANOVA followed by post hoc analysis with Scheffe's test (StatView software, Abacus Concepts Inc., Berkeley, CA) and P values <0.05 were considered significant.

Acknowledgments

This study was partly supported by grants-in-aid for scientific research from the Ministry of Education, Culture, Sports, Science and Technology of Japan for AH and by research grant for intractable diseases (vestibular disorders) from the Ministry of Health, Labor and Welfare of Japan for TK. We thank Dr. Kalubi Bukasa for critical reading of the manuscript.

REFERENCES

Abel, T., Martin, K.C., Bartsch, D., Kandel, E.R., 1998. Memory suppressor genes: inhibitory constraints on the storage of long-term memory. Science 279, 338–341.

Balaban, C.D., Freilino, M., Romero, G.G., 1999. Protein kinase C inhibition blocks the early appearance of vestibular compensation. Brain Res. 845, 97–101.

Beaumont, V., Zhong, N., Fletcher, R., Froemke, R.C., Zucker, R.S., 2001. Phosphorylation and local presynaptic protein synthesis in calcium- and calcineurin-dependent induction of crayfish long-term facilitation. Neuron 32, 489–501.

Belmeguenai, A., Hansel, C., 2005. A role for protein phosphatases 1, 2A, and 2B in cerebellar long-term potentiation. J. Neurosci. 25, 10768–10772.

Butcher, S.P., Henshall, D.C., Teramura, Y., Iwasaki, K., Sharkey, J., 1997. Neuroprotective actions of FK506 in experimental stroke: in vivo evidence against an antiexcitotoxic mechanism. J. Neurosci. 17, 6346–6939.

Carafoli, E., 1994. Biogenesis: plasma membrane calcium ATPase: 15 years of work on the purified enzyme. FASEB J. 8, 993–1002.

Curthoys, I.S., Halmagyi, G.M., 1995. Vestibular compensation: a

review of the ocular motor, neural and clinical consequences of unilateral vestibular loss. J. Vestibular Res. 5, 67–107.
Darlington, C.L., Smith, P.F., 1992. Pre-treatment with a Ca^{2+} channel antagonist facilitates vestibular compensation. NeuroReport 3, 143–145.
Darlington, C.L., Smith, P.F., 1996. The recovery of static vestibular function following peripheral vestibular lesions in mammals: the intrinsic mechanism hypothesis. J. Vestibular Res. 6, 185–201.
Dieringer, N., 1995. Vestibular compensation-neural plasticity and its relations to functional recovery after labyrinthine lesions in frogs and other vertebrates. Prog. Neurobiol. 46, 97–129.
Fukudo, M., Yano, I., Masuda, S., Okuda, M., Inui, K., 2005. Distinct inhibitory effects of tacrolimus and cyclosporine A on calcineurin phosphatase activity. J. Pharmacol. Exp. Ther. 312, 816–825.
Gilchrist, D.P., Darlington, C.L., Smith, P.F., 1993. Effects of flunarizine on ocular motor and postural compensation following peripheral vestibular deafferentation in the guinea pig. Pharmacol. Biochem. Behav. 44, 99–105.
Gold, B.G., Katoh, K., Storm-Dickerson, T., 1995. The immunosuppressant FK506 increases the rate of axonal regeneration in rat sciatic nerve. J. Neurosci. 15, 7509–7516.
Him, A., Dutia, M.B., 2001. Intrinsic excitability changes in vestibular nucleus neurons after unilateral deafferentation. Brain Res. 908, 58–66.
Horii, A., Smith, P.F., Darlington, C.L., 2001. Quantitative changes in gene expression of glutamate receptor subunits/subtypes in the vestibular nucleus, inferior olive and flocculus before and following unilateral labyrinthectomy in the rat: real-time quantitative PCR method. Exp. Brain Res. 139, 188–200.
Horii, A., Smith, P.F., Darlington, C.L., 2002. Application of real-time quantitative polymerase chain reaction to quantification of glutamate receptor gene expression in the vestibular brainstem and cerebellum. Brain Res. Protoc. 9, 77–83.
Horii, A., Kitahara, T., Smith, P.F., Darlington, C.L., Masumura, C., Kubo, T., 2003. Effects of unilateral labyrinthectomy on GAD, GAT1 and GABA receptor gene expression in the rat vestibular nucleus. NeuroReport 14, 2359–2363.
Horii, A., Masumura, C., Smith, P.F., Darlington, C.L., Kitahara, T., Uno, A., Mitani, K., Kubo, T., 2004. Microarray analysis of gene expression in the rat vestibular nucleus complex following unilateral vestibular deafferentation. J. Neurochem. 91, 975–982.
Kerr, D.R., Sansom, A.J., Smith, P.F., Darlington, C.L., 2000. Comparison of protein kinase activity and protein phosphorylation in the medial vestibular nucleus and prepositus hypoglossi in labyrinthine-intact and labyrinthectomized guinea pigs. J. Vestibular Res. 10, 107–117.
Leinhos, P., Flohr, H., 1992. Ca^{2+} antagonists and lesion-induced plasticity. Eur. J. Neurosci., Suppl. 5, 74.
Lisman, J., 1989. A mechanism for the Hebb and the anti-Hebb processes underlying learning and memory. Proc. Natl. Acad. Sci. U. S. A. 86, 9574–9578.
Mansuy, I.M., 2003. Calcineurin in memory and bidirectional plasticity. Biochem. Biophy. Res. Comm. 311, 1195–1208.
Ochiishi, T., Yamauchi, T., Terashima, T., 1998. Regional differences between the immunohistochemical distribution of Ca^{2+}/calmodulin-dependent protein kinase II alpha and beta isoforms in the brainstem of the rat. Brain Res. 790, 129–140.
Ris, L., Capron, B., Nonclercq, D., Alexandre, H., Sindic, C., Toubeau, G., Godaux, E., 2003. Labyrinthectomy changes T-type calcium channels in vestibular neurones of the guinea pig. NeuroReport 14, 1585–1589.
Sansom, A.J., Brent, V.A., Jarvie, P.E., Darlington, C.L., Smith, P.F., Laverty, R., Rostas, J.A., 1997. In vitro phosphorylation of medial vestibular nucleus and prepositus hypoglossi proteins during behavioural recovery from unilateral vestibular deafferentation in the guinea pig. Brain Res. 778, 166–177.
Sansom, A.J., Smith, P.F., Darlington, C.L., Laverty, R., 2000. The effects of protein kinase C and calmodulin kinase II inhibitors on vestibular compensation in the guinea pig. Brain Res. 882, 45–54.
Serafin, M., de Waele, C., Khateb, A., Vidal, P.P., Muhlethaler, M., 1991. Medial vestibular nucleus in the guinea-pig: II. Ionic basis of the intrinsic membrane properties in brainstem slices. Exp. Brain Res. 84, 426–433.
Sharkey, J., Butcher, S.P., 1994. Immunophilins mediate the neuroprotective effects of FK506 in focal cerebral ischaemia. Nature 371, 336–339.
Smith, P.F., Curthoys, I.S., 1989. Mechanisms of recovery following unilateral labyrinthectomy: a review. Brain Res. Rev. 14, 155–180.
Tanaka, C., Saito, N., 1992. Localization of subspecies of protein kinase C in the mammalian central nervous system. Neurochem. Int. 21, 499–512.
Tolu, E., Mameli, O., Caria, M.A., Melis, F., 1988. Improvement of vestibular plasticity in the guinea pig with a calcium entry blocker. Acta Oto-laryngol. Suppl. 460, 72–79.
Ueno, T., Kameyama, K., Hirata, M., Ogawa, M., Hatsuse, H., Takagaki, Y., Ohmura, M., Osawa, N., Kudo, Y., 2002. A mouse with a point mutation in plasma membrane Ca^{2+}-ATPase isoform 2 gene showed the reduced Ca^{2+} influx in cerebellar neurons. Neurosci. Res. 42, 287–297.
Usachev, Y.M., Toutenhoofd, S.L., Goellner, G.M., Strehler, E.E., Thayer, S.A., 2001. Differentiation induces up-regulation of plasma membrane Ca^{2+}-ATPase and concomitant increase in Ca^{2+} efflux in human neuroblastoma cell line IMR-32. J. Neurochem. 76, 1756–1765.
Vibert, N., Babalian, A., Serafin, M., Gasc, J.P., Muhlethaler, M., Vidal, P.P., 1999. Plastic changes underlying vestibular compensation in the guinea-pig persist in isolated, in vitro whole brain preparations. Neuroscience 93, 413–432.
Xia, Z., Storm, D.R., 2005. The role of calmodulin as a signal integrator for synaptic plasticity. Nat. Rev., Neurosci. 6, 267–276.
Yang, Y., Fischer, Q.S., Zhang, Y., Baumgartel, K., Mansuy, I.M., Daw, N.W., 2005. Reversible blockade of experience-dependent plasticity by calcineurin in mouse visual cortex. Nat. Neurosci. 8, 791–796.

The Laryngoscope
Lippincott Williams & Wilkins, Inc.

Novel Method for Recording Vestibular Evoked Myogenic Potential: Minimally Invasive Recording on Neck Extensor Muscles

Koichi Sakakura, MD, PhD; Katsumasa Takahashi, MD, PhD; Yukihiro Takayasu, MD, PhD; Kazuaki Chikamatsu, MD, PhD; Nobuhiko Furuya, MD, PhD

Objectives: **Vestibular evoked myogenic potential (VEMP) has been used to test vestibulocollic reflex. However, VEMP is not stable on elderly patients because of their weak muscular strength. In this study, we tried to record VEMP on median neck extensor muscles with weak muscular contraction** ***Study Design:*** **We recorded VEMP from normal subjects and patients by novel and conventional methods** ***Method:*** **Thirty-one normal subjects and 56 patients with vertigo or hearing loss were tested in a seated or prone position without muscular tension. The different electrodes were placed on the median surface at the palpable bottom of the occipital bone** ***Results:*** **Our response showed a clear negative peak at 13 ms on normal subjects, with reversed polarity compared with VEMP on the sternocleidomastoid muscle. This potential is defined as VEMP caused by the proper latencies, dependency of the strength on sound stimulation, and independence of hearing ability. In the cases of acoustic neurinoma, onset latencies were prolonged or nonexistent. The responses on neck extensor muscles could not be recorded on some elderly patients.** ***Conclusion:*** **This new method of recording VEMP is less invasive and suitable for elderly patients.** ***Key Words:*** **Vestibular evoked myogenic potential (VEMP), neck extensor muscles, elderly patients, acoustic neurinoma.**

Laryngoscope, **115:1768–1773, 2005**

From the Department of Otolaryngology–Head and Neck Surgery, Gunma University Graduate School of Medicine, Maebashi, Gunma, Japan.

Editor's Note: This Manuscript was accepted for publication May 27, 2005.

This work was supported in part by a Grant-in-Aid for General Scientific Research (B) 16390484, a Grant-in-Aid for General Scientific Research (C) 17591775, and a Grant-in-Aid for Young Scientists 17791158, Ministry of Education, Science, Sports and Culture, Japan.

Send Correspondence to Nobuhiko Furuya, Department of Otolaryngology–Head and Neck Surgery, Gunma University Graduate School of Medicine, 3-39-22 Showa-Machi, Maebashi, Gunma, 371-8511, Japan. E-mail: nfuruya@med.gunma-u.ac.jp

DOI: 10.1097/01.mlg.0000173157.34039.d8

INTRODUCTION

Several muscle responses in the human neck elicited by acoustic stimulation are known; the acoustic startle reflex is one of them. The circuit of the reflex is thought to consist of the cochlear nucleus, dorsal or ventral lateral lemniscus, reticularis pontis caudalis, and head or spinal motoneurons.[1–3] The inion response, originally recorded between inion (medial occipital region) and nose by Bickford and Cody et al.[4–6] in 1964, suggested that the mechanism of this response was a neck muscular response elicited by sound stimuli by way of the vestibular system. The inion response was thought to be of saccular origin because the response was recorded in both healthy subjects and patients with hearing or vestibular disorders. However, this unstable response was not used clinically as a parameter of vestibular function. Colebatch et al.[7] reported vestibular evoked myogenic potential (VEMP) derived from the saccule. VEMP is widely used as a test of vestibular function, especially the function of the saccular or inferior vestibular nerve. However, it is difficult to record VEMP for the majority of elderly patients because a stable record of VEMP requires proper muscular tension.

VEMP is generally acquired at the sternocleidomastoid muscle (SCM). On the other hand, some investigators recorded the myogenic potential evoked by click at the trapezius muscle and the splenius capitis muscle.[8–10] All these responses and the inion response require strong muscular tension to obtain sufficient amplitude. Therefore, these responses are not suitable for elderly patients and patients in the acute phase of a vertigo attack. In this study, we attempted to arrange the previously reported method to establish the new recording with weaker, noninvasive muscular tension.

SUBJECTS AND METHODS

Subjects

Thirty-one normal subjects (20–39 years old, 20 males and 11 females) and 56 patients with vertigo or hearing loss (HL)

(18–79 years old, 25 males and 31 females) were examined. These cases included 18 cases of acoustic neurinoma, 9 cases of Ménière's disease, 8 cases of severe deafness, 5 cases of sudden deafness, and 4 cases of vestibular neuritis were enrolled in this study. The characteristics of the patients in this study are presented in Table I.

VEMP Recordings

The recordings were performed in a soundproofed and shielded room. The subjects were seated in chairs without fixation of the head, or they were in the prone position on beds, according to Wu et al.[10] The different electrodes were placed on the median surface at the palpable bottom of the occipital bone (inion), namely at the origin of neck extensors, and on the surface of the bilateral splenius capitis muscles, the middle point between the mastoid process, and the spinous process of C7. The electrodes placed in the hair were fixed with circular nets. The reference electrode was placed on the surface of the spinous process of C7. A median frontal electrode was used as the ground (Fig. 1). The subjects were instructed to relax their bodies, and they were not required to contract their neck muscles. Short tone bursts (500 Hz, rise/fall = 1 ms, plateau = 2 ms) with a recurrence frequency of 5 Hz were presented to a unilateral ear by way of closed ear headphones, and the contralateral ear was masked by band-pass noise. The stimulated side was regarded as the ipsilateral side in our median neck extensor recording. The responses were filtered between 20 Hz and 2 kHz, averaged over 200 sweeps by Neuropack MEB-2200 (Nihon-Koden, Tokyo, Japan). VEMP on the SCM of each subject was recorded by the same stimulation conditions. Namely, the different electrodes were placed on the upper half of the SCM with a reference electrode on the upper middle end of the sternum. The subjects were required to contract the SCM as much as possible during the recording with electromyographic monitoring.

Simultaneously, inion response was recorded according to Cody et al.[5] The different electrodes were placed on the median surface at the inion. The reference electrode was placed on the nose. Subjects were seated with or without backward neck tension, stimulated by short tone burst or long tone burst (105 dB, 500 Hz, rise/fall = 1 ms, plateau = 10 ms).

TABLE I.
Profile of Patients.

Characteristics	No. of Patients
Acoustic neurinoma	17
Ménière's disease	9
Idiopathic deafness	8
Sudden deafness	6
Vestibular neuritis	4
Unknown vertigo	4
Benign paroxysmal positional vertigo	1
Hunt syndrome	1
Large vestibular aqueduct syndrome	1
Vertebrobasilar insufficiency	1
Brainstem tumor	1
Brainstem infarction	1
Spinocerebellar ataxia	1
Cerebellar hemangioma	1

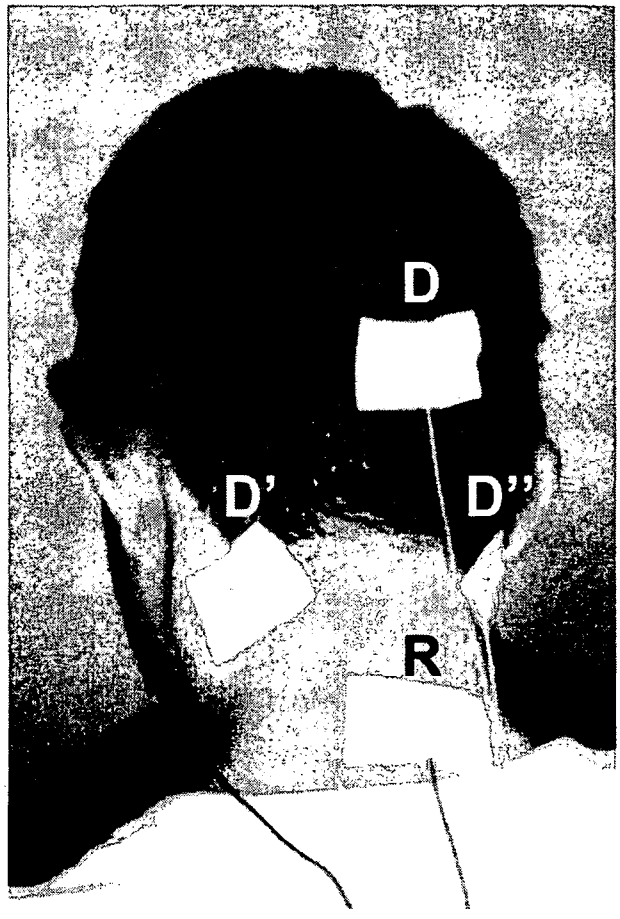

Fig. 1. Position of the electrodes for recording the neck extensor vestibular evoked myogenic potential (VEMP). The different electrodes were placed on the median surface at the palpable bottom of the occipital bone (inion, D), and on the surface of the bilateral splenius capitis muscles, the middle point between the mastoid process, and the spinous process of C7 (D', D''). The reference electrode was placed on the surface of the spinous process of C7 (R).

Ultrasonographic Measurement

Ultrasonographic measurement for the rear neck was conducted in 14 normal subjects. Thicknesses of subcutaneous tissue including fat and neck extensor muscles were measured.

Caloric Test

Caloric test by cold water was performed for each patient with vertigo or HL. Bilateral maximum slow phase velocities (degree/s) were measured by Video-Oculography (2D-VOG system, Interacoustic, Assens, Denmark). Canal paresis percent (CP%) was defined as the difference of bilateral maximum slow phase velocities for convenience.

Visual and Median Nerve Stimulation

Four normal subjects were stimulated by visual and electrical stimuli to distinguish the vestibular response from nonspecific response. Subjects had their head positioned in a forward or backward direction.

For the recording of visual evoked potential (VEP), we placed the different electrode 5 cm above the inion and the reference electrodes on the bilateral postauricles, whose potentials

were summated through the amplifier. Two types of photic stimulations were used for VEP recording: a strobe flash triggered by SLS-3100 (Nihon Koden, Tokyo, Japan) and pattern reversal stimulation programmed in Neuropack MEB-2200. The strobe was placed 1 m in front of the subjects with a 0.6 J intensity. The duration of the flash was 10 s presented at a rate of 2 Hz. Pattern reversal stimulation was displayed on a 17 inch monitor 1 m in front of the subjects, presented at a rate of 2 Hz. The visual angle (θ) was 14.3 degrees.

For the recording of short latency somatosensory evoked potential (SSEP) using the median nerve, the different electrodes were placed on the forehead (FPZ), 7 cm to the left and 2 cm below the top of the head (C4'), on the bilateral median clavicle (EP1/EP2) and the spinous process of C5 (C5S). The potential differences between C4' and FPZ, C4' and EP2, C5S and FPZ, EP1 and EP2 were used for evaluation of SSEP. We placed the stimulating electrodes on the left median nerve at the distal forearm and the ground electrodes proximally to the stimulating electrodes. The intensity of the stimulus varied from 4.5 to 5.5 mA, which was necessary to cause a distinct twitch of the thumb. The duration of the electric shock was 1 millisecond presented at a rate of 2 Hz.

Statistical Analysis

A Mann-Whitney U test was performed for statistical analysis of thickness in subcutaneous tissue. $P < .05$ was considered to be significant.

RESULTS

Neck Extensor Response

Figure 2 shows the myogenic potential on the median neck extensor of a normal subject. The mean onset latency, the period of time from the stimulation to the beginning of the response, of the neck extensor response at 105 dB SPL stimulation was 10.80 ms (SD ±0.71); the negative peak appeared at 13.30 ms (SD ±1.16) in normal controls. The mean amplitude of the responses was 7.46 μV (SD 4.79). However, the monitored electromyograms (Fig. 3A) that were sufficient to elicit the response were obviously smaller than that of VEMP on SCM (Fig. 3B). The comparison of the parameters between responses on the neck extensor and on the SCM is summarized in Table II.

The median thresholds of sound stimuli on the neck extensor response was 95 dB SPL (SD 4.24), ranging from

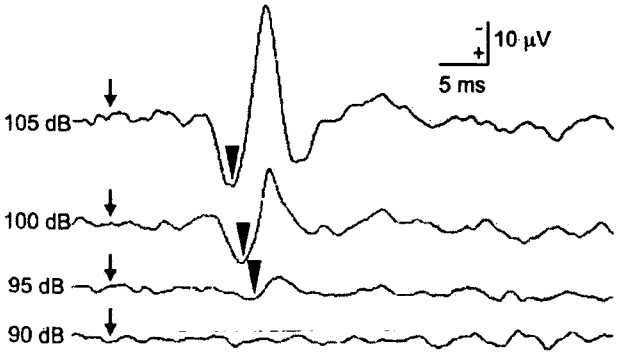

Fig. 2. Myogenic potential on the median neck extensor of a normal subject. Threshold of sound stimuli for appearance was 95 dB SPL. Triangles indicate the onset latency.

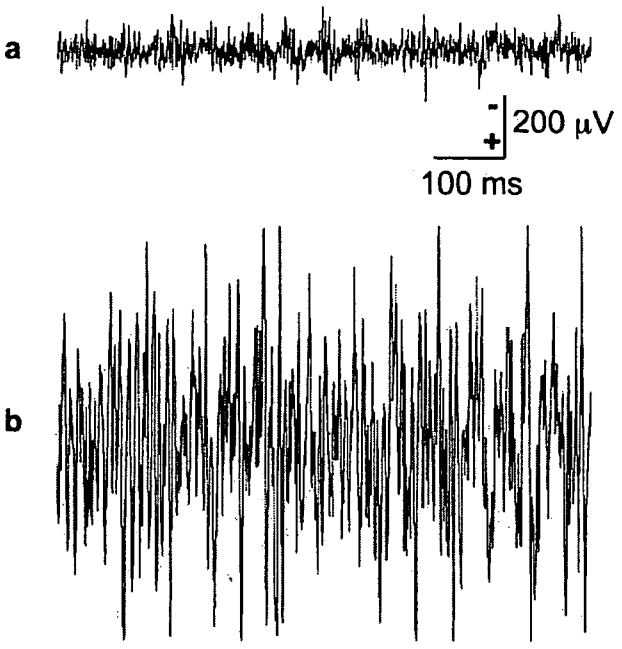

Fig. 3. Background activities of the muscles during the recording of the response on neck extensor muscles (A) and vestibular evoked myogenic potential (VEMP) on sternocleidomastoid muscle (SCM) (B). The response on neck extensor muscles required smaller muscular tension than VEMP on SCM.

90 to 105 dB. The monitored electromyogram and the recorded negative response at the median neck extensor were larger in amplitude than those on the splenius capitis muscle (Fig. 4). The potentials recorded had a larger amplitude when the subjects were in the prone position versus the seated position (data not shown). When the neck extensors were completely relaxed, no response was recorded on the muscles (data not shown). The response was recorded in only 5 (45.5%) of the 11 cases aged over 70 years old. The percentage of appearance of the response and VEMP on SCM in young normal subjects, patients, and elderly patients is presented in Table III.

Neck extensor response showed a lower percentage of appearance than VEMP in young normal subjects and total patients; however, the response showed a similar percentage to VEMP on SCM in elderly patients over 70 years old, regardless of small background tension in the neck muscles.

TABLE II.
Parameters of Vestibular Evoked Myogenic Potential on Neck Extensor and Sternocleidomastoid Muscle (SCM).

	Neck Extensor (n = 23)	SCM (n = 23)
Onset latency (ms)	10.80 (SD = 0.71)	8.97 (SD = 0.74)
1st peak latency (ms)	13.30 (SD = 1.16)	13.14 (SD = 0.85)
2nd peak latency (ms)		21.49 (SD = 2.74)
1st peak amplitude (V)	7.46 (SD = 4.79)	58.62 (SD = 28.51)
2nd peak amplitude (V)		61.72 (SD = 49.00)

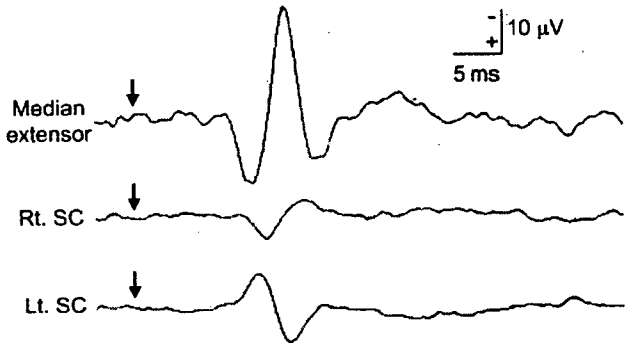

Fig. 4. The negative responses at the median neck extensor were larger in amplitude than those on the bilateral splenius capitis muscle (SC). The right side was stimulated.

Figure 5 shows various neck extensor responses in the cases of acoustic neurinoma. Six (35.3%) of 17 responses in the disease side were nonexistent (Fig. 5A). Three (17.6%) of 17 cases showed responses on the disease side; however, the onset latencies of all responses were prolonged (Fig. 5B). The appearance of the neck extensor response in acoustic neurinoma cases has no correlation with CP%. CP% in the disease ear that had no neck extensor response varied from 3% to 63%, whereas CP% in the disease ear that had incomplete extensor response varied from 3% to 82%. The neck extensor response in the cases of Ménière's disease also varied and, therefore, could not be evaluated; however, the CP% of these cases were very small (<10%). Three to four cases of vestibular neuritis lacked bilateral neck extensor responses and VEMP on SCM. The remaining case of vestibular neuritis had bilateral normal neck extensor responses and VEMP on SCM; however, CP% was 75%. Two to six sudden deafness cases presented with normal neck extensor response in the disease sides. CP% of these 2 cases was 11% and 16%. Three to 13 complete deaf ears also presented normal responses. These ears, which had deafness and normal neck extensor response, had normal maximum slow phase velocities in caloric test.

The median thickness of subcutaneous tissue of subjects that presented with neck extensor response measured by ultrasonograph is 3.8 mm (n = 10, SD 1.43). The median thickness of subcutaneous tissue of subjects that have an absent neck extensor response is 4.15 mm (n = 4, SD 2.35). There is no significant difference between these two groups.

TABLE III.
Percentage of Appearance of Vestibular Evoked Myogenic Potential on Neck Extensor and Sternocleidomastoid Muscle (SCM).

	Neck Extensor (%)	SCM (%)
Young normal subjects (n = 31) (20–39, mean 25.5 years)	74.2	92.0
Patients* (n = 56) (18–79, mean 57.4 years)	53.6	61.5
Aged patients over 70 years* (n = 11) (71–79, mean 74.5 years)	45.5	45.5

*Percentage of appearance in probable healthy side.

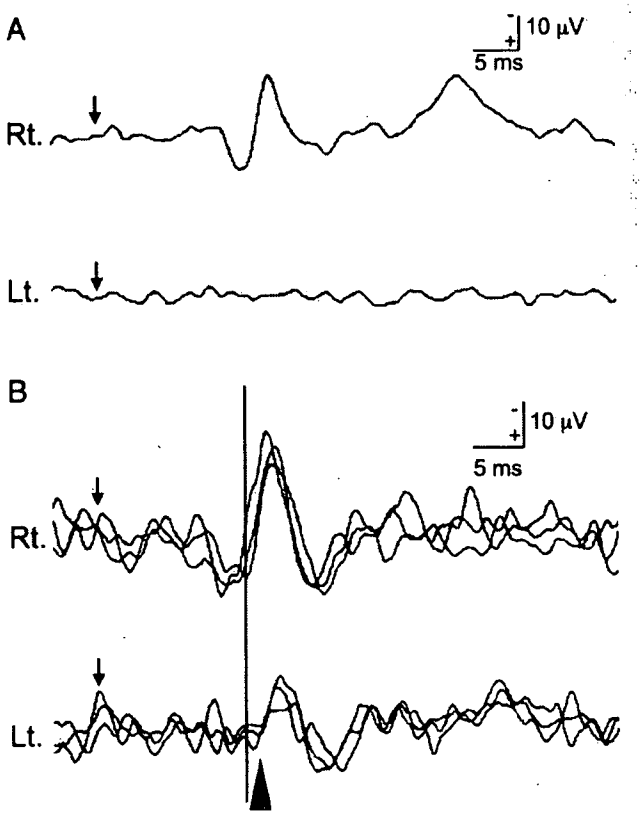

Fig. 5. Various neck-extensor responses in patients with acoustic neurinoma. (A) Median neck extensor response of a 61-year-old-male with left acoustic neurinoma. Response to the right stimulation presented a typical negative wave, whereas the left response to ipsilateral stimulation was nonexistent. (B) Neck-extensor response of a 51-year-old male with left acoustic neurinoma. In the affected side (Lt) the responses appeared; however, the onset latencies in the disease side were prolonged compared with the healthy side (triangle).

Visual and Electrical Stimulation

Next, we recorded neck-extensor response, inion response, and VEP or SSEP for various stimulations such as tone burst, strobe, pattern reversal, and electrical stimulation to the median nerve. We recognized neck extensor response and inion response simultaneously elicited by tone-burst stimulation with negative neck position (Fig. 6). In contrast, the neck extensor response and the inion response at approximately 13 ms did not appear when the photic stimulation and electrical stimulation to the median nerve were given with negative neck tension. However, although VEP and SSEP were successfully presented when subjects were seated or rested, these response nonexistent or were lost in myogenic noises when the subjects exerted negative tension on their necks (data not shown).

DISCUSSION

VEMP is not useful for elderly patients or patients in an acute or subacute stage of a vertigo attack because of

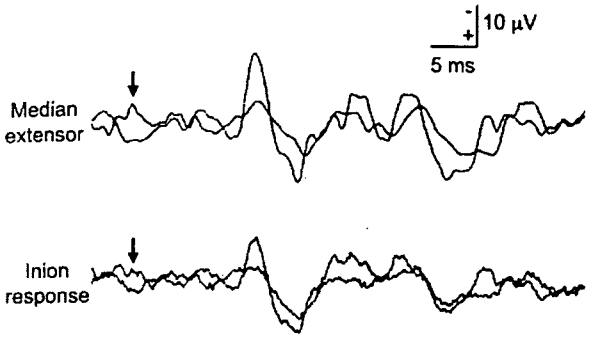

Fig. 6. Simultaneous recording of the median neck extensor response and inion response. The wave patterns resembles each other.

its dependence on muscle tension, although it is a useful examination for evaluating vestibular function. Nevertheless, recordings of VEMP in a prone position were attempted with sufficient muscular contraction in previous studies, and the obtained responses were weak or disturbed by noise.[8–10] We obtained stable recording of the response elicited by a tone burst on the neck extensor muscle without voluntary muscle contraction in this study. This responses were defined as VEMP based on the following properties: 1) the threshold of the response was higher than that of hearing over 60 dB, 2) the response depended on muscle tension, 3) the response was weakened or nonexistent in patients with disorder of the vestibular nerve such as an acoustic tumor, and 4) the latency of the negative peak was similar to the first peak of VEMP (p13) on SCM. The onset latency and peak latency of the response were more stable than those of the postauricular response and the inion response that Cody et al. [4–6] reported previously. The onset latency of the negative wave of the postauricular response in normal subjects varied from 7 to 24 (mean 10) ms, and the peak latency ranged from 10 to 32 (mean 15) ms. The onset latency of a wave of the inion response in normal subjects varied from 6.5 to 12 (mean 8.8) ms, and the peak latency ranged from 10 to 19 (mean 14.1) ms.[6] On the other hand, the onset latency of the response in our study varied from 9.6 to 11.9 (mean 10.8, .D ±0.71) ms, and the peak latency ranged from 10.5 to 15.5 (mean 13.3, SD ±1.16) ms. The latency of our responses that we recorded was stable, and the mean latency is considered to correspond to p13 of VEMP on SCM (Table II). The onset latency especially, not the peak latency, is parallel to stimulation strength;[11] the onset latency in our data are more stable than the postauricular response and the inion response that was previously reported.[6] Previous data reported that the onset latency of the startle reflex in humans ranged from 14 to 151 ms,[3] and the reflex shows habituation in proportion to frequent stimuli. Our response had shorter latency compared with the startle reflex. Moreover, habituation was not observed in the present study. Therefore, the difference between the startle reflex and the response in our study is obvious.

VEMP on SCM is presented with a positive (p13)/negative (n23) pattern. Ferber-Viart et al.[8] reported that click-evoked potential on trapezius muscle also showed positive/negative pattern with similar latencies. However, the response on neck extensors recorded in this study showed opposite polarity, with a negative peak at 13 ms. Another article reported that the corresponding response showed a negative/positive pattern at the latency of 13 ms.[10] Uchino et al.[12] reported that electrical stimulation to the saccular nerve elicited inhibitory postsynaptic potentials predominantly in ipsilateral neck flexor muscle motoneurons and elicited excitatory postsynaptic potentials predominantly in ipsilateral neck extensor motoneurons in the sacculocollic reflex. Recently, we recorded VEMP presenting with negative/positive pattern in rat neck extensor.[11] These physiologic data explain the reversal polarity in VEMP between the neck flexor and extensor.

The weak point of our median neck VEMP is a low appearance when comparing VEMP with SCM. However, our VEMP on the neck extensor required little muscular tension, whereas VEMP on SCM required the strong load, and its percentage of appearance was good. Especially, we were able to present a similar percentage of VEMP on the neck extensor and SCM in elderly patients despite little tension of the neck extensor muscle. This technique appears to be suitable for elderly patients with vertigo, who cannot generate strong muscular contractions. We measured the thickness of the subcutaneous tissue including fat and neck extensor muscles, however, because no correlation was found between the appearance of the response and the thickness of the subcutaneous tissue. We postulate that other factors are related to the unstable appearance of this response.

The neck extensor response and inion response had a close recording site and were synchronized at 13 ms in onset latencies and polarities (Fig. 5). VEMP and inion responses have been considered to come from the same origin.[13] The present responses we recorded on neck extensor muscle correspond to the inion response. However, our recording method is simple and easy compared with the other methods used on the posterior neck, including the inion response. We also tried to record another evoked responses, VEP and SSPE, because Cody and Bickford[6] reported that the inion response, especially at the late phase, was evoked by light-flash and electric-shock stimulation. We did not succeed in simultaneous recording of VEMP on median neck extensors and VEP or SSEP with neck tension. The neck extensor VEMP is not supposed to be a part of VEP or SSEP. Moreover, the response at 13 ms was not a nonspecific response because of the absence of elicitation by light or electrical stimulation.

Furthermore, we could record the neck extensor response in patients with severe sensory HL or who were deaf. It appears the nature of VEMP is as Colebatch et al.[7] reported previously. In addition, patients with acoustic neurinoma have shown prolonged onset latencies or absence of VEMP on the median neck extensor. Some investigators demonstrated that most acoustic neurinoma grows at the inferior vestibular nerve,[14,15] from which VEMP would predominantly originate. Interestingly, we could present the prolongation of the onset latency of VEMP on neck extensor in all patients with acoustic neurinoma who showed a response in the affected ear. Moreover, we also confirmed the prolongation of the onset

latency of VEMP on SCM (preliminary data). We tried to investigate simultaneously CP% using a caloric test in cases of acoustic neurinoma, but there was no correlation between the appearance of VEMP on neck extensor and CP% because the caloric test mainly reflects the function of the superior vestibular nerve.[16]

CONCLUSION

The VEMP recording method on the median neck extensor at inion described here is less invasive than conventional VEMP recording methods because of slight muscular contraction. This method is expected to be useful for defining vestibular ability in patients with weak muscular contraction.

BIBLIOGRAPHY

1. Lee Y, Lopez DE, Meloni EG, Davis M. Aprimary acoustic startle pathway: obligatory role of cochlear root neuronsand the nucleus reticularis pontis caudalis. *J Neurosci* 1996;16:3775–3789.
2. Pellet J. Neural organization in the brainstem circuit mediating the primary acoustic head startle: an electrophysiological study in the rat. *Physiol Behav* 1990;48:727–739.
3. Yeomans JS, Frankland PW. The acoustic startle reflex: neurons and connections. *Brain Res Rev* 1996;21:301–314.
4. Bickford RG, Jacobson JL, Cody DT. Nature of average evoked potentials to sound and other stimuli in man. *Ann N Y Acad Sci* 1964;112:204–223.
5. Cody DT, Jacobson JL, Walker JC, Bickford RG. Averaged evoked myogenic and cortical potentials to sound in man. *Ann Otol Rhinol Laryngol* 1964;73:763–777.
6. Cody DT, Bickford RG. Averaged evoked myogenic responses in normal man. *Laryngoscope* 1969;79:400–416.
7. Colebatch JG, Halmagyi GM, Skuse NF. Myogenic potentials generated by a click-evoked vestibulocollic reflex. *J Neurol Neurosurg Psychiatry* 1994;57:190–197.
8. Ferber-Viart C, Duclaux R, Colleaux B, Dubreuil C. Myogenic vestibular-evoked potentials in normal subjects: a comparison between responses obtained from sternomastoid and trapezius muscles. *Acta Otolaryngol (Stockh)* 1997;117: 472–481.
9. Ferber-Viart C, Soulier N, Dubreuil C, Duclaux R. Cochleovestibular afferent pathways of trapezius muscle responses to clicks in human. *Acta Otolaryngol (Stockh)* 1998;118:6–10.
10. Wu C, Young Y, Murofushi T. Tone burst-evoked myogenic potentials in human neck flexor and extensor. *Acta Otolaryngol (Stockh)* 1999;119:741–744.
11. Sakakura K, Miyashita M, Chikamatsu K, et al. Tone burst-evoked myogenic potentials in rat neck extensor and flexor muscles. *Hear Res* 2003;185:57–64.
12. Uchino Y, Sato H, Sasaki M, et al. Sacculocollic reflex arcs in cats. *J Neurophysiol* 1997;77:3003–3012.
13. Ferber-Viart C, Dubreuil C, Duclaux R. Vestibular evoked myogenic potentials in humans: a review. *Acta Otolaryngol (Stockh)* 1999;119:6–15.
14. Ylikoski J, Palva T, Collan Y. Eighth nerve in acoustic neuromas. Special reference to superior vestibular nerve function and histopathology. *Arch Otolaryngol* 1978;104: 532–537.
15. Clemis JD, Ballad WJ, Baggot PJ, Lyon ST. Relative frequency of inferior vestibular schwannoma. *Arch Otolaryngol Head Neck Surg* 1986;112:190–194.
16. Aw ST, Haslwanter T, Fetter M, et al. Contribution of the vertical semicircular canals to the caloric nystagmus. *Acta Otolaryngol (Stockh)* 1998;118:618–627.

Cellular/Molecular

CD47 Promotes Neuronal Development through Src- and FRG/Vav2-Mediated Activation of Rac and Cdc42

Takaaki Murata,[1,2] Hiroshi Ohnishi,[1] Hideki Okazawa,[1] Yoji Murata,[1] Shinya Kusakari,[1] Yuriko Hayashi,[1] Motoaki Miyashita,[1] Hiroshi Itoh,[3] Per-Arne Oldenborg,[4] Nobuhiko Furuya,[2] and Takashi Matozaki[1]

[1]Laboratory of Biosignal Sciences, Institute for Molecular and Cellular Regulation, Gunma University, Maebashi, Gunma 371-8512, Japan, [2]Department of Otolaryngology, Gunma University Graduate School of Medicine, Gunma 371-8511, Japan, [3]Department of Cell Biology, Graduate School of Biological Sciences, Nara Institute of Science and Technology, Ikoma, Nara 630-0192, Japan, and [4]Department of Integrative Medical Biology, Section for Histology and Cell Biology, Umeå University, S-901 87 Umeå, Sweden

The development of axons and dendrites is controlled by small GTP-binding proteins of the Rho family, but the upstream signaling mechanisms responsible for such regulation remain unclear. We have now investigated the role of the transmembrane protein cluster of differentiation 47 (CD47) in this process with hippocampal neurons. CD47-deficient neurons manifested markedly impaired development of dendrites and axons, whereas overexpression of CD47 promoted such development. Interaction of SH2 domain-containing protein tyrosine phosphatase substrate-1 (SHPS-1) with CD47 also induced the formation of dendritic filopodia and spines. These effects of CD47 were prevented by inhibition of either cell division cycle 42 (Cdc42) or Rac. In CD47-deficient neurons, autophosphorylation of Src was markedly reduced. In addition, overexpression of CD47 promoted the autophosphorylation of Src. Inhibition of Src family kinases indeed prevented CD47-promoted dendritic development. Inhibition of either FGD1-related Cdc42-guanine nucleotide exchange factor (GEF) (FRG) or Vav2, which is a GEF for Cdc42 and Rac and is activated by Src, also prevented the effects of CD47 on dendritic development. These results indicate that CD47 promotes development of dendrites and axons in hippocampal neurons in a manner dependent, at least in part, on activation of Cdc42 and Rac mediated by Src as well as by FRG and Vav2.

Key words: dendrite; Src; small GTP-binding protein; guanine nucleotide exchange factor; SHPS-1; hippocampus

Introduction

Regulation of the extension and branching of axons and dendrites is essential for the formation of functional neuronal networks in the mammalian CNS. Such regulation is achieved by a variety of extracellular signaling molecules, including diffusible factors, extracellular matrix proteins, and cell adhesion molecules (Tessier-Lavigne and Goodman, 1996; Dickson, 2002; Jan and Jan, 2003). In response to such extracellular signals, axons or dendrites produce or retract filopodia or lamellipodia, actions that require the temporal and spatial regulation of the actin cytoskeleton. Members of the Rho family of small GTP-binding proteins, including Rho, Rac, and cell division cycle 42 (Cdc42), are implicated as key mediators that link extracellular signals to rearrangement of the actin cytoskeleton in neurons (Luo et al., 1997; Takai et al., 2001; Govek et al., 2005). Indeed, certain neuronal guidance factors, including slit, semaphorin, and ephrin, have been shown to regulate Rho family proteins (Polleux et al., 2000; Wahl et al., 2000; Shamah et al., 2001; Whitford et al., 2002). However, the mechanisms responsible for integration of other extracellular signals, such as those generated by adhesion molecules, with Rho family proteins in the promotion of axonal and dendritic development remain poorly understood.

Cluster of differentiation 47 is a member of the Ig superfamily of proteins, possessing an IgV-like extracellular region, five putative transmembrane domains, and a short cytoplasmic tail (Brown and Frazier, 2001). CD47 is expressed throughout the brain (Reinhold et al., 1995), being especially abundant in synapse-rich regions such as the molecular layer and synaptic glomeruli of the cerebellum, the plexiform layers of the retina, and the hippocampus (Jiang et al., 1999; Mi et al., 2000; Ohnishi et al., 2005), and its expression increases markedly during postnatal development (Mi et al., 2000; Ohnishi et al., 2005). In addition, the abundance of CD47 mRNA in the hippocampus correlates with memory retention in rats (Huang et al., 1998), and long-term potentiation is impaired in CD47-deficient mice (Chang et al., 1999), suggesting that CD47 plays a role in synaptic plasticity and memory formation in the hippocampus. However, the precise function of CD47 in neurons and its mode of action at the molecular level remain essentially unknown.

We have shown recently that forced expression of CD47 promotes neurite formation in N1E-115 neuroblastoma cells in a

Received June 6, 2006; accepted Oct. 13, 2006.

This work was supported by a Grant-in-Aid for Scientific Research on Priority Areas Cancer, a Grant-in-Aid for Scientific Research on Priority Areas Molecular Brain Science, a grant of the 21st Century COE Program from the Ministry of Education, Culture, Sports, Science, and Technology of Japan, Swedish Research Council Grant 31X-14286, National Institutes of Health Grant GM57573-06, and grants from the Swedish Society of Medicine and the Faculty of Medicine, Umeå University, Sweden. We thank Y. Takai, M. Okada, M. Matsuda, and J. Miyazaki for reagents, as well as H. Kobayashi, K. Tomizawa, and Y. Niwayama for technical assistance.

Correspondence should be addressed to Takashi Matozaki, Laboratory of Biosignal Sciences, Institute for Molecular and Cellular Regulation, Gunma University, 3-39-15 Showa-Machi, Maebashi, Gunma 371-8512, Japan. E-mail: matozaki@showa.gunma-u.ac.jp.

DOI:10.1523/JNEUROSCI.3981-06.2006

 0270-6474/06/2612397-11$15.00/0

manner dependent on the activation of Rac and integrin β3 (Miyashita et al., 2004). Indeed, the extracellular region of CD47 associates with integrin β3 or β1 subunits, and most CD47-mediated responses in non-neuronal cells, such as migration of neutrophils and activation of platelets, appear to require integrin activation (Brown and Frazier, 2001). Moreover, we also shown that forced expression of CD47 or exposure to a recombinant fusion protein of SHPS-1 (SH2 domain-containing protein tyrosine phosphatase substrate-1) and the Fc domain of Ig markedly promoted Cdc42-mediated filopodium formation in N1E-115 neuroblastoma cells (Miyashita et al., 2004). SHPS-1, also known as BIT (brain Ig-like molecule with tyrosine-based activation motifs) or SIRPα (signal-regulatory protein α), is a ligand for the extracellular region of CD47 (Jiang et al., 1999). It is a transmembrane protein that contains three Ig-like domains in its extracellular region as well as putative tyrosine phosphorylation sites and binding sites for the Src homology 2 domains of the protein tyrosine phosphatase SHP-2 (SH2 domain-containing protein tyrosine phospatase) in its cytoplasmic region (Fujioka et al., 1996; Ohnishi et al., 1996). SHPS-1 is expressed throughout the brain, and the regions in which it is especially abundant overlap in large part with those in which CD47 is also concentrated (Mi et al., 2000; Ohnishi et al., 2005). In addition, we have shown recently that SHPS-1 and CD47 are preferentially localized to axons and dendrites, respectively, in cultured hippocampal neurons (Ohnishi et al., 2005). Together, these observations suggest that CD47 promotes neurite formation and that the interaction of SHPS-1 with CD47 mediates directional intercellular communication between axons and dendrites.

We here examined whether CD47, through its interaction with SHPS-1, indeed promotes dendritic or axonal development in hippocampal neurons *in vitro* and *in vivo*. Furthermore, we investigated the intracellular signals that might mediate such actions of CD47 in neurons.

Materials and Methods

Animals. $CD47^{+/-}$ mice were described previously (Lindberg et al., 1996) and were crossed to obtain litters of CD47-deficient ($CD47^{-/-}$) and wild-type (WT) ($CD47^{+/+}$) animals. Mice were bred and maintained under specific pathogen-free conditions at the Institute of Experimental Animal Research of Gunma University.

Primary antibodies and reagents. A rat monoclonal antibody (mAb) to mouse CD47 (miap 301) was obtained from PharMingen (San Diego, CA). A mouse mAb to the Flag epitope (M2) was from Sigma (St. Louis, MO). Rhodamine-conjugated phalloidin was from Invitrogen (Carlsbad, CA), rabbit polyclonal antibodies (pAbs) to C-terminal Src kinase (Csk) were from Santa Cruz Biotechnology (Santa Cruz, CA), and rabbit pAbs to microtubule-associated protein 2 (MAP2) were from Chemicon (Temecula, CA). 4-Amino-5-(4-chlorophenyl)-7-(t-butyl)pyrazolo[3,4-d]pyrimidine (PP2) and 4-amino-7-phenylpyrazol[3,4-d]primidine (PP3), a mouse mAb to Src (Ab-1), and a mouse mAb to tau1 were obtained from Calbiochem (La Jolla, CA). Rabbit pAbs to the Tyr^{416}-phosphorylated form of Src were from Cell Signaling Technology (Danver, MA). A mouse mAb to the Myc epitope (9E10) was purified from the culture supernatant of hybridoma cells. Rabbit pAbs to CD47 were prepared as described previously (Miyashita et al., 2004). Rabbit pAbs to mouse FGD1-related Cdc42-guanine nucleotide exchange factor (GEF) (FRG) were generated by injection of rabbits with a synthetic peptide antigen (EPEQSLSPRMQEKHC), of which the sequence corresponded to amino acids 30–40 of mouse FRG; the pAbs were purified from rabbit serum by affinity chromatography with the peptide antigen conjugated to Sepharose. SHPS-1–Fc was prepared as described previously (Miyashita et al., 2004).

Plasmids. Expression vectors for mouse CD47 form 4 and green fluorescent protein (GFP)–β-actin were described previously (Miyashita et al., 2004). Plasmids encoding Myc–RacT17N, Myc–neuronal Wiskott-Aldrich syndrome protein (NWASP)–Cdc42/Rac-interactive binding region (CRIB), Myc–Vav2–WT, Myc–Vav2–dominant negative (DN), Flag–FRG–WT, or Flag–FRG–ΔDHPH were kindly provided by Y. Takai (Osaka University, Osaka, Japan). A plasmid encoding full-length mouse FRG was obtained from American Type Culture Collection (Manassas, VA) (MGC-6304), and a plasmid encoding myr–Csk, which contains a myristylation signal at its NH_2 terminus, was kindly provided by M. Okada (Osaka University). The cDNAs contained in these plasmids were subcloned in the pCAGGS vector, which was kindly provided by J. Miyazaki (Osaka University). Plasmids encoding Raichu–Rac1 or Raichu–Cdc42 were kindly provided by M. Matsuda (Osaka University).

Determination of dendritic and axonal morphology. Hippocampal neurons (3×10^5 per 35 mm dish) were isolated from newborn mice [postnatal day 0 (P0) to P1] and plated on culture dishes coated with poly-D-lysine (25 μg/ml) as described previously (Miyashita et al., 2004). The neurons were transfected with expression vectors for GFP–actin and CD47 (as well as with additional expression vectors as indicated) with the use of LipofectAMINE2000 (Invitrogen); transfection was performed the day after plating [1 d *in vitro* (DIV)] or at 4 DIV. At 3–21 DIV, neurons were fixed for 20–30 min at room temperature with PBS containing 4% paraformaldehyde and 0.1% glutaraldehyde and were then permeabilized for 60 min at room temperature with PBS containing 0.1% Triton X-100 and 5% goat serum. They were incubated for 1 h at room temperature or overnight at 4°C with primary antibodies diluted in the permeabilization solution, washed with PBS, and then incubated for 1 h at room temperature with secondary antibodies conjugated with cyanine 3 (Jackson ImmunoResearch, West Grove, PA), Alexa488 (Invitrogen), or aminomethylcoumarin acetate (Jackson ImmunoResearch). For staining of filamentous actin, neurons were incubated with rhodamine-conjugated phalloidin. The cells were finally washed with PBS and examined with a confocal laser-scanning microscope (LSM5 Pascal; Zeiss, Oberkochen, Germany) or an Olympus Optical (Tokyo, Japan) AX-70 microscope. The morphology of transfected neurons was examined with the fluorescence signal of GFP–actin. In other experiments, neurons were cultured at low density (4×10^4 per 35 mm dish) without forced expression of GFP–actin, and the morphology of dendrites or axons was examined by immunostaining for the dendritic marker MAP2 or the axonal marker tau1. The length of axons and dendrites was measured with the use of software of the LSM5 Pascal microscope and was integrated to obtain the total length of these neurites. The number of branches of each axon was quantified by counting the corresponding number of terminal tips.

Quantitation of filopodia and spines. Mouse hippocampal neurons cultured on dishes coated with poly-D-lysine (25 μg/ml) and either control human IgG or SHPS-1–Fc were transfected with expression vectors as described above. Neurons were fixed at 3–21 DIV, and cell morphology was examined by monitoring of GFP–actin fluorescence with the LSM5 Pascal microscope. To quantify the numbers of dendritic filopodia and spines, we classified dendritic protrusions labeled with GFP–actin as filopodia or spines according to the following morphological criteria: (1) a headless protrusion with a length of >0.5 μm and <8 μm and with a length/width ratio of >2 was classified as a filopodium; (2) all dendritic protrusions with a length of >0.5 μm and <8 μm other than filopodia were classified as spines.

Immunoprecipitation and immunoblot analysis. Cultured hippocampal neurons (1×10^6 per 35 mm dish) were washed with ice-cold PBS and then lysed on ice in 1 ml of lysis buffer (20 mM Tris-HCl, pH 7.6, 140 mM NaCl, 1 mM EDTA, and 1% NP-40) containing 1 mM phenylmethylsulfonyl fluoride, aprotinin (10 μg/ml), and 1 mM sodium vanadate. The lysates were centrifuged at 21,000 × *g* for 15 min at 4°C, and the resulting supernatants were subjected to immunoprecipitation and immunoblot analysis as described previously (Fujioka et al., 1996; Miyashita et al., 2004).

RNA interference. Two expression vectors, siRNAfrg–GFP#1 and siRNAfrg–GFP#2, which each encode an FRG small interfering RNA (siRNA) and enhanced GFP (EGFP), were constructed. Two 19 nt sequences (5′-CTCAGAAACAACTAGTAGA-3′ and 5′-GGAATTT-ACTAGCTACTTC-3′) corresponding to nucleotides 1138–1156 and 2000–2018 of mouse FRG mRNA (GenBank accession number

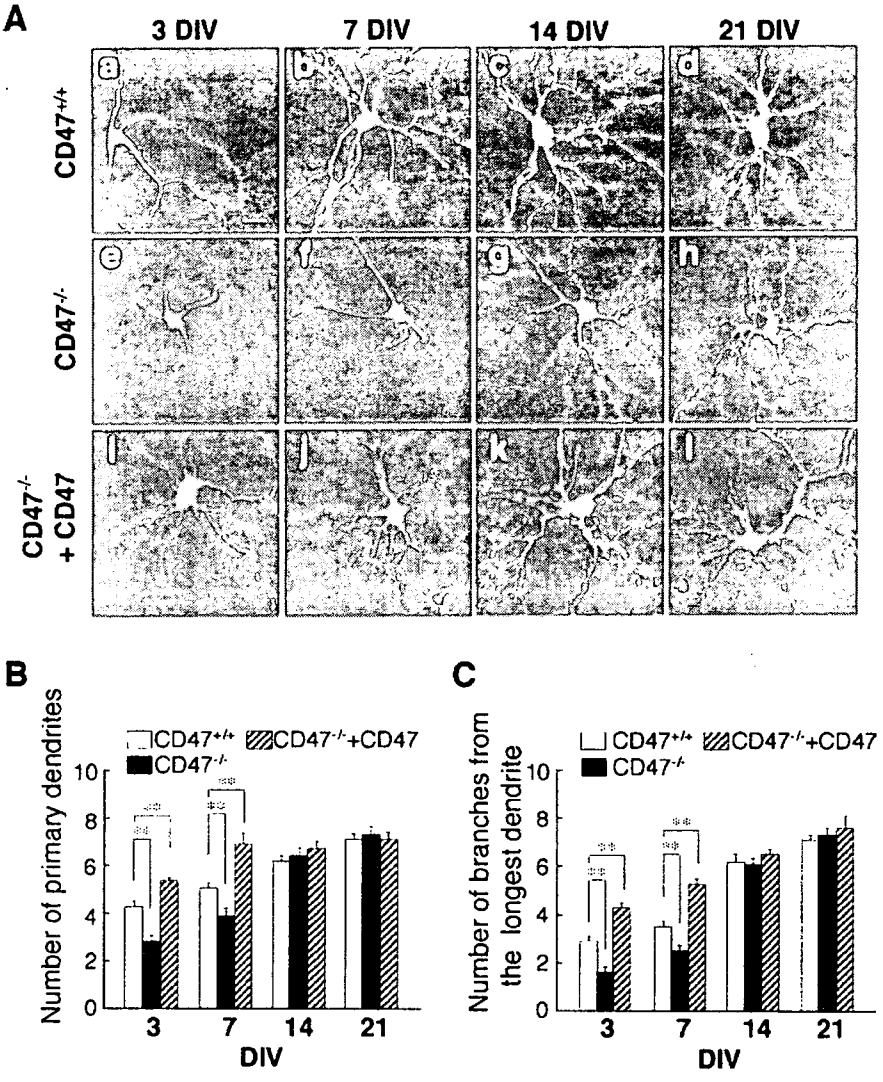

Figure 1. Impairment of dendritic development in cultured hippocampal neurons from *CD47*$^{-/-}$ mice. ***A***, Hippocampal neurons isolated from newborn WT (*CD47*$^{+/+}$) (***a–d***) or *CD47*$^{-/-}$ (***e–l***) mice were transfected with an expression vector for GFP–actin and either an expression vector for CD47 (***i–l***) or the corresponding empty vector (***a–h***) at 1 DIV (***a***, ***e***, ***i***) or 4 DIV (***b–d***, ***f–h***, ***j–l***). Neurons were fixed at 3 DIV (***a***, ***e***, ***i***), 7 DIV (***b***, ***f***, ***j***), 14 DIV (***c***, ***g***, ***k***), or 21 DIV (***d***, ***h***, ***l***), and the morphology of each neuron as revealed by GFP–actin was examined by fluorescence microscopy. Scale bar, 20 μm. ***B***, ***C***, Neurons treated as in ***A*** were evaluated for their dendritic morphology at the indicated times. The numbers of primary dendrites per neuron (***B***) and of branches from the longest primary dendrite of each neuron (***C***) were determined for *CD47*$^{+/+}$ neurons (open columns), *CD47*$^{-/-}$ neurons (filled columns), and *CD47*$^{-/-}$ neurons expressing ectopic CD47 (hatched columns). Data are means ± SE of values obtained from a total of 28–36 neurons in three independent experiments. $^{**}p < 0.01$ (Student's *t* test) for the indicated comparisons.

NM145519) were selected for construction of the siRNAfrg–GFP vectors, which direct the synthesis of the corresponding 19 bp double-stranded target sequence. Two pairs of 64 nt sequences, each of which contains a targeting sequence and its reverse complementary sequence (pair 1, 5′-GATCCCCCTCAGAAACAACTAGTAGATTCAAGAGATCTACTAGTTGTTTCTGAGTTTTTGGAAA-3′ and 5′-AGCTTTTCCAAAAACTCAGAAACAACTAGTAGATCTCTTGAATCTACTAGTTGTTTCTGAGGGG-3′; pair 2, 5′-GATCCCCGGAATTTACTAGCTACTTCTTCAAGAGAGAAGTAGCTAGTAAATTCCTTTTTGGAAA-3′ and 5′-AGCTTTTCCAAAAAGGAATTTACTAGCTACTTCTCTCTTGAAGAAGTAGCTAGTAAATTCCGGG-3′), were synthesized. After an annealing step, each pair of oligonucleotides was inserted into the pSUPER vector (Brummelkamp et al., 2002). The resulting vectors, pSUPER–mFRG#1 and pSUPER–mFRG#2, were digested with *Kpn*I and *Sac*I, and the released DNA fragment containing the H1 promoter and downstream short-hairpin sequence was rendered blunt-ended and subcloned into the blunted *Sal*I site of the EGFP expression vector pCAGGS–EGFP. The resulting vectors were designated siRNAfrg–GFP#1 and siRNAfrg–GFP#2.

Fluorescent resonance energy transfer analysis. The fluorescence resonance energy transfer (FRET) imaging was performed as described previously (Itoh et al., 2002). In brief, primary cultured mouse hippocampal neurons were co-transfected with expression vectors for CD47 (or the corresponding empty vector) and either Raichu–Rac1 or Raichu–Cdc42 at 1 DIV. Forty-eight hours after transfection (at 3 DIV), the cells were fixed and stained with mAb to CD47 to confirm the expression of exogenous CD47. FRET images were acquired on the Aquacosmos/Ashura system (Hamamatsu Photonics, Shizouka, Japan) using an IX-81 inverted microscope equipped with a UPlanApo 100×, 1.35 numerical aperture oil-immersion objective (Olympus Optical), a 440AF21 excitation filter, a 455DRLP dichroic mirror, a 460ALP emission filter, and a three CCD color camera (C7780-22; Hamamatsu Photonics). Image acquisition and analysis were performed using Aquacosmos 2.6 software (Hamamatsu Photonics).

Results

Impaired development of dendrites and axons in hippocampal neurons of CD47-deficient mice

We have shown recently that the abundance of CD47 in dendrites is greater than that in axons of cultured hippocampal neurons (Ohnishi et al., 2005). To evaluate the possible role of CD47 in the regulation of neuronal development, we prepared cultures of hippocampal neurons from WT and *CD47*$^{-/-}$ mice (Lindberg et al., 1996) and then determined the numbers of primary dendrites, which are derived directly from the cell body, in these neurons.

As described previously (Ohnishi et al., 2005), the expression of CD47 in hippocampal neurons isolated from newborn WT mice was apparent at only a low level after 3 DIV but had increased markedly by 7 DIV (see Fig. 3*Ae*,*Ag*). Such expression was not detected in neurons prepared from *CD47*$^{-/-}$ mice (supplemental Fig. 1, available at www.jneurosci.org as supplemental material). To examine the morphology of individual neurons in detail, we transfected the cells with an expression vector for a fusion protein containing GFP and β-actin at 1 or 4 DIV and then cultured them further for various times (Fig. 1). The number of primary dendrites on each *CD47*$^{-/-}$ neuron at 3 or 7 DIV was markedly smaller than that apparent for WT neurons (Fig. 1*A*). Quantitative analysis revealed that this difference was statistically significant (Fig. 1*B*). For this analysis, a primary dendrite was defined as a process derived directly from the cell body with a length equal to or greater than one-half of the diameter of the cell body (~8 μm) and with a diameter of >2 μm.

We also examined the effect of CD47 deficiency on the branching of dendrites by counting the total number of branches derived from the longest primary dendrite of each neuron. A

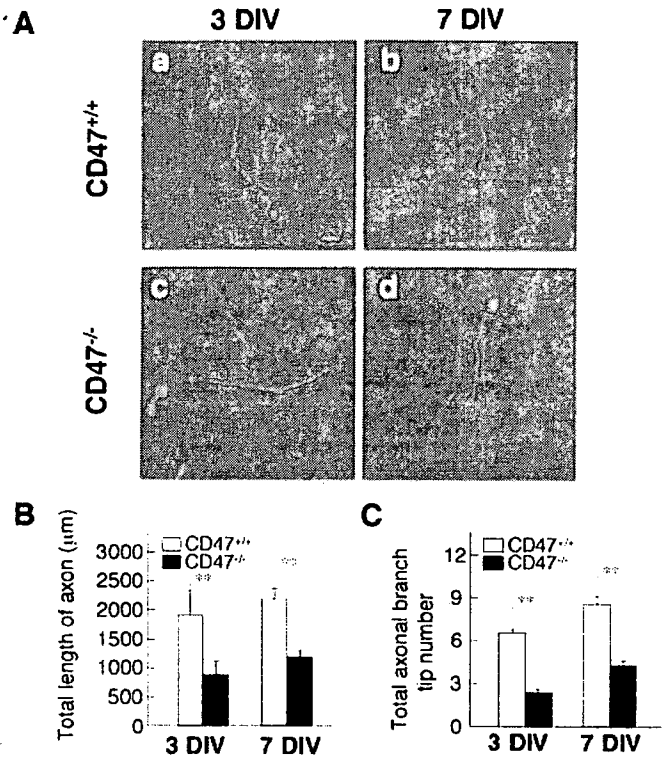

Figure 2. Impairment of axonal development in cultured hippocampal neurons from *CD47*$^{-/-}$ mice. *A*, Cultured hippocampal neurons from *CD47*$^{+/+}$ (*a*, *b*) or *CD47*$^{-/-}$ (*c*, *d*) mice were fixed at 3 DIV (*a*, *c*) or 7 DIV (*b*, *d*) and stained with an mAb to tau1. Scale bar, 20 μm. *B*, *C*, The length of the primary axon (*B*) and the number of terminal branch tips for the primary axon (*C*) were determined for neurons cultured and stained as in *A*. Data are means ± SE of values obtained from a total of 28 neurons in three independent experiments. $^{**}p < 0.01$ (Student's *t* test).

branch was defined as a process whose length was at least equal to one-half of the diameter of the cell body. Quantitative analysis revealed that the number of branches originating from the longest primary dendrite of *CD47*$^{-/-}$ neurons was also significantly decreased at 3 or 7 DIV compared with that apparent for WT neurons (Fig. 1*C*). In contrast, the number of primary dendrites or that of branches from the longest primary dendrite did not differ between *CD47*$^{-/-}$ and WT neurons at 14 or 21 DIV (Fig. 1).

We also examined the morphology of hippocampal neurons cultured at low density without transfection and stained with pAbs to MAP2, a dendritic marker protein. We measured the total length of all dendrites and their branches in the neurons at 3 and 7 DIV. The total length of dendrites was markedly reduced in *CD47*$^{-/-}$ neurons compared with WT neurons at both time points (supplemental Fig. 2*A*,*B*, available at www.jneurosci.org as supplemental material). The numbers of primary, secondary, and tertiary dendritic branches were also markedly reduced in *CD47*$^{-/-}$ neurons at 3 or 7 DIV compared with those for WT neurons (supplemental Fig. 2*A*,*C*, available at www.jneurosci.org as supplemental material). In addition, the number of branches from the longest primary dendrite was also substantially decreased in *CD47*$^{-/-}$ neurons at either 3 or 7 DIV compared with that for WT neurons (data not shown).

We next examined the effect of CD47 deficiency on axon morphology by staining cultured hippocampal neurons with an mAb to tau1, an axon marker protein (Fig. 2). The length of the primary axon of *CD47*$^{-/-}$ neurons was significantly smaller than that for WT neurons at 3 or 7 DIV (Fig. 2*A*,*B*). We also counted the number of terminal tips derived from each primary axon to determine the extent of axonal branching; this parameter was also markedly reduced for *CD47*$^{-/-}$ neurons at 3 or 7 DIV compared with that for WT neurons (Fig. 2*C*). In addition, the percentage of neurons that manifested an enlarged growth cone (a growth cone with four or more filopodia and with lamellipodia; other growth cones were considered to be collapsed) at the most distal end of the primary axon was significantly smaller for *CD47*$^{-/-}$ neurons (45.2 ± 5.09%; $n = 500$ neurons) than for WT neurons (63.8 ± 6.91%; $n = 500$ neurons; $p = 0.014$, Student's *t* test) at 4 DIV. Together, these data suggested that CD47 is required for proper development of both dendrites and axons in cultured hippocampal neurons during the first few (3–7) DIV. However, it may not be required for additional development of dendrites at later stages (14–21 DIV).

Effects of forced expression of CD47 on dendrite development

The development of dendrites and axons was markedly impaired in hippocampal neurons of *CD47*$^{-/-}$ mice. We therefore next examined the effect of forced expression of CD47 on the morphology of hippocampal neurons of WT mice. For these experiments, we focused on the contribution of CD47 to dendritic development because the morphology of dendrites is more readily determined than is that of axons, which are highly elongated and manifest multiple and complex branching patterns. One of four alternatively spliced isoforms of CD47 (form 4) predominates in the brain (Reinhold et al., 1995). We therefore transfected hippocampal neurons cultured at high density with expression vectors for mouse CD47 (form 4) and GFP–actin at 1 or 4 DIV and examined the morphology of the neurons at 3–21 DIV. The expression of endogenous CD47 in hippocampal neurons from WT mice was detected at a relatively low level at 3 DIV (Fig. 3*Ae*). Transfection with the CD47 vector resulted in marked increases in both the abundance of this protein (Fig. 3*Af*,*Ah*) and the number of primary dendrites apparent at 3 or 7 DIV (Fig. 3*A*,*B*). Forced expression of CD47 also increased the number of branches from the longest primary dendrite at these time points (Fig. 3*C*). However, the number of primary dendrites or that of branches from the longest primary dendrite did not differ between the neurons overexpressing CD47 and mock-transfected neurons at 14 or 21 DIV (Fig. 3*B*,*C*).

We also examined the effect of forced expression of CD47 on dendrite development in *CD47*$^{-/-}$ neurons. Expression of CD47 in *CD47*$^{-/-}$ neurons reversed the decreases in the numbers of primary dendrites and of branches from the longest primary dendrite apparent in these cells at 3 or 7 DIV (Fig. 1*Ai*–*Al*); indeed, these parameters in the *CD47*$^{-/-}$ neurons expressing CD47 were significantly increased compared with those for WT neurons (Fig. 1*B*,*C*).

Effects of an SHPS-1–Fc fusion protein and forced expression of CD47 on the formation of dendritic filopodia and spines

The development of dendrites is accompanied by the extension of filopodia, which form contacts with synaptic terminals of axons and then mature into dendritic spines (Ziv and Smith, 1996). We have shown previously that SHPS-1–Fc, an Fc fusion protein containing the extracellular region of the CD47 ligand SHPS-1, promoted filopodium formation in N1E-115 neuroblastoma cells and that this effect was enhanced by overexpression of CD47 (Miyashita et al., 2004). We therefore next examined the effects of SHPS-1–Fc and forced expression of CD47 on the formation of

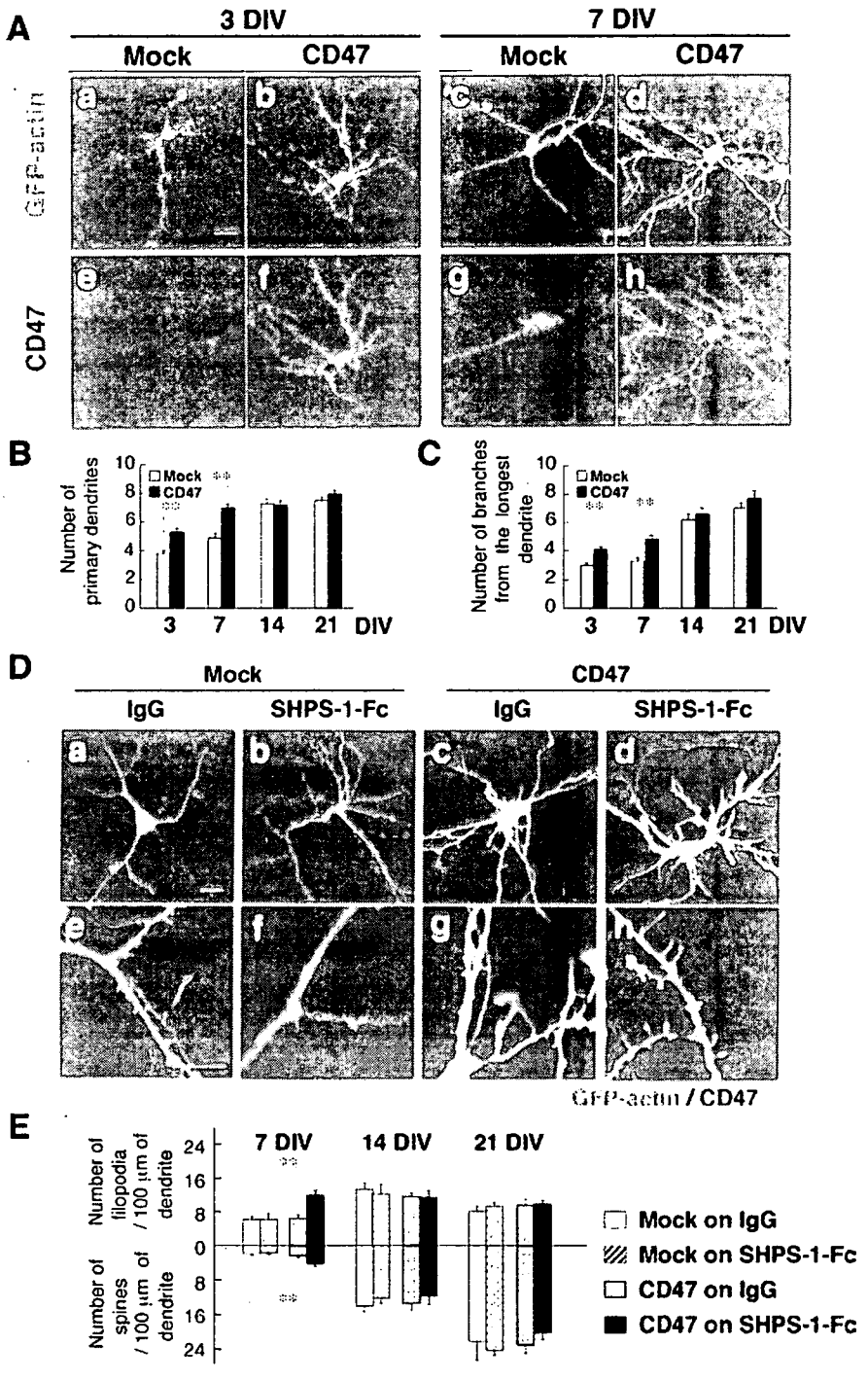

Figure 3. Effects of SHPS-1–Fc and forced expression of CD47 on dendrite development and the formation of filopodia and spines. ***A***, Hippocampal neurons from WT mice were transfected with an expression vector for GFP–actin and either a vector for CD47 (***b***, ***d***, ***f***, ***h***) or the corresponding empty vector (***a***, ***c***, ***e***, ***g***) at 1 DIV (***a***, ***b***, ***e***, ***f***) or 4 DIV (***c***, ***d***, ***g***, ***h***). Neurons were fixed at 3 DIV (***a***, ***b***, ***e***, ***f***) or 7 DIV (***c***, ***d***, ***g***, ***h***) and stained with an mAb to CD47 (***e***–***h***). Fluorescence images of GFP–actin were also obtained (***a***–***d***). Scale bar, 20 μm. ***B***, ***C***, The number of primary dendrites per neuron (***B***) and that of branches from the longest primary dendrite of each neuron (***C***) were determined for cells treated as in ***A*** and cultured for the indicated times. Data are means ± SE of values obtained from a total of 22–30 neurons in three independent experiments. $^{**}p < 0.01$ (Student's *t* test). ***D***, Hippocampal neurons from WT mice were cultured on dishes coated with SHPS-1–Fc (***b***, ***d***, ***f***, ***h***) or control human IgG (***a***, ***c***, ***e***, ***g***) and were transfected at 4 DIV with a vector for GFP–actin and either a vector for CD47 (***c***, ***d***, ***g***, ***h***) or the corresponding empty vector (***a***, ***b***, ***e***, ***f***). Neurons were fixed and stained with an mAb to CD47 (red) as well as monitored for GFP–actin fluorescence (green) at 7 DIV. Scale bar, 20 μm. ***E***, The densities of dendritic filopodia and spines at 7, 14, and 21 DIV were determined for neurons treated as in ***D***. Data are means ± SE of values obtained from a total of 18–24 neurons in three independent experiments. $^{**}p < 0.01$ (Student's *t* test).

dendritic filopodia and spines in hippocampal neurons of WT mice.

We classified dendritic protrusions labeled with GFP–actin as filopodia or spines on the basis of morphological characteristics proposed in a previous study (Takahashi et al., 2003) and as described in Materials and Methods. At 7 DIV, the number of dendritic filopodia was greater than that of spines (Fig. 3*D*,*E*). The numbers of these structures were approximately equal at 14 DIV, and the number of spines was greater than that of filopodia at 21 DIV (Fig. 3*E*), consistent with previous observations (Takahashi et al., 2003). Neither SHPS-1–Fc nor forced expression of CD47 alone affected the formation of filopodia or spines at 7–21 DIV (Fig. 3*D*,*E*). In contrast, the combination of SHPS-1–Fc and forced expression of CD47 resulted in a significant increase in the numbers of both filopodia and spines at 7 DIV compared with those apparent for mock-transfected neurons plated on control human IgG (Fig. 3*D*,*E*). Such effects were not apparent at 14 or 21 DIV (Fig. 3*E*). We also examined the effects of SHPS-1–Fc and forced expression of CD47 on dendrite development in cultured hippocampal neurons. SHPS-1–Fc alone failed to increase the number of primary dendrites or that of branches from the longest primary dendrite in mock-transfected neurons at 7 DIV (supplemental Fig. 3, available at www.jneurosci.org as supplemental material). In addition, SHPS-1–Fc did not further increase the number of primary dendrites or that of branches from the longest primary dendrite in CD47-overexpressing neurons at 7 DIV (supplemental Fig. 3, available at www.jneurosci.org as supplemental material).

Role of Rac and Cdc42 in dendritic development promoted by CD47

We next investigated the intracellular signaling pathway responsible for the stimulatory effect of CD47 on dendritic development. Hippocampal neurons from WT mice were transfected with expression vectors for GFP–actin, CD47, and either a dominant-negative mutant of Rac1 (RacT17N) or the CRIB domain of NWASP (NWASP–CRIB) at 4 DIV and were examined for their morphology at 7 DIV. Immunostaining confirmed that individual neurons were successfully transfected with the combination of three different plasmids (supplemental Fig. 4, available at www.jneurosci.org as supplemental material). Forced expression of Myc epitope-tagged RacT17N in the ab-

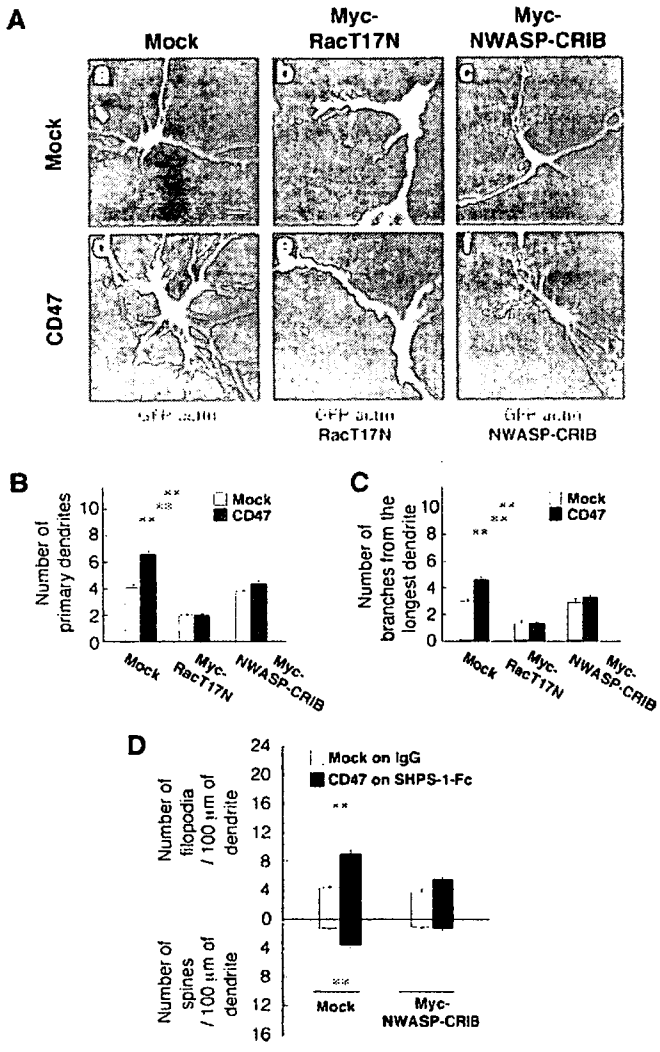

Figure 4. Participation of Rac and Cdc42 in the promotion of dendritic development by forced expression of CD47. ***A***, Hippocampal neurons from WT mice were transfected at 4 DIV with an expression vector for GFP–actin, a CD47 vector (***d–f***) or the corresponding empty vector (***a–c***), and either a vector for Myc epitope-tagged RacT17N (***b***, ***e***) or Myc–NWASP–CRIB (***c***, ***f***) or the corresponding empty vector (***a***, ***d***). At 7 DIV, the neurons were fixed and stained with an mAb to Myc (red), and GFP–actin fluorescence was also monitored (green). Neurons were also stained with an mAb to CD47 to confirm its overexpression (data not shown; see supplemental Fig. 3, available at www.jneurosci.org as supplemental material). Scale bar, 20 μm. ***B***, ***C***, The number of primary dendrites per neuron (***B***) and that of branches from the longest primary dendrite of each neuron (***C***) were determined for neurons treated as in ***A***. Data are means ± SE of values obtained from a total of 30 neurons in three independent experiments. $^{**}p < 0.01$ (Student's *t* test). ***D***, Hippocampal neurons from WT mice were plated on dishes coated with SHPS-1–Fc or control human IgG and were transfected at 4 DIV with a vector for GFP–actin, a vector for CD47 or the corresponding empty vector, and a vector for Myc epitope-tagged NWASP–CRIB or the corresponding empty vector. At 7 DIV, the neurons were fixed and stained with an mAb to Myc, and the densities of dendritic filopodia and spines were determined. Data are means ± SE of values obtained from a total of 30 neurons in three independent experiments. $^{**}p < 0.01$ (Student's *t* test).

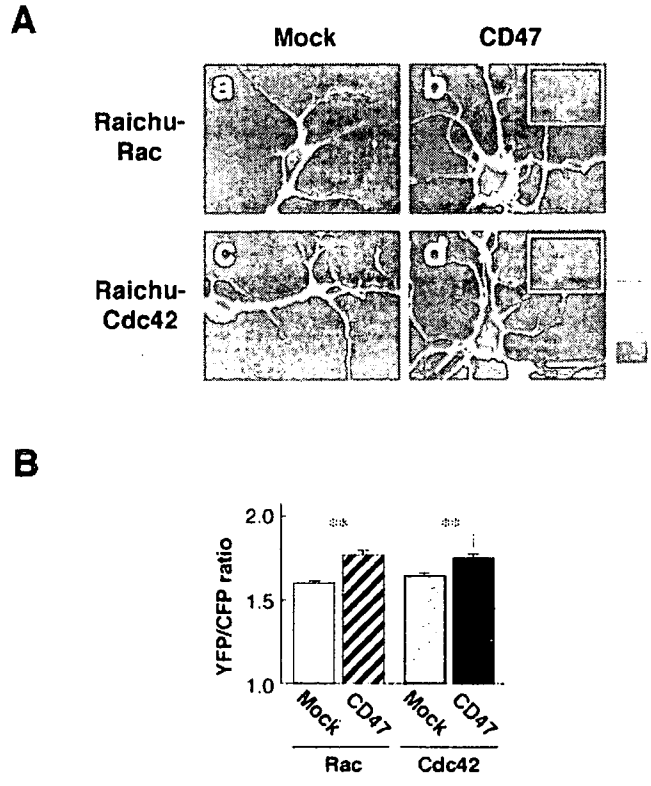

Figure 5. Activation of Rac and Cdc42 by forced expression of CD47 in hippocampal neurons. ***A***, Hippocampal neurons from WT mice were transfected with an expression vector for CD47 (***b***, ***d***) (or the corresponding empty vector (Mock; ***a***, ***c***) and a vector for either Raichu–Rac (***a***, ***b***) or Raichu–Cdc42 (***c***, ***d***) at 1 DIV. Neurons were fixed at 3 DIV and stained with mAb to CD47 to confirm the expression of CD47 (shown in insets in ***b*** and ***d***). The images of YFP/CFP ratio of transfected neurons were shown in the intensity-modulated display mode. In the intensity-modulated display mode, eight colors from red to blue are used to represent the YFP/CFP ratio, with each color indicating the mean intensity of YFP/CFP ratio. The upper and lower limits of the ratio image are shown on the right. Scale bar, 20 μm. ***B***, YFP/CFP ratios in dendrites were quantified in transfected neurons. Data are means ± SE of values from eight neurons and are representative of three independent experiments. $^{**}p < 0.01$ (Student's *t* test).

sence of that of CD47 resulted in marked increases in the diameter of primary dendrites and in the formation of filopodia at the margin of these dendrites (Fig. 4*Ab*). Furthermore, expression of RacT17N prevented the increases in both the number of primary dendrites and branches from the longest primary dendrite induced by forced expression of CD47, although it also reduced these parameters in neurons not overexpressing CD47 (Fig. 4*Ab*,*Ae*,*B*,*C*). NWASP–CRIB specifically binds the GTP-bound (active) form of Cdc42 and thereby inhibits its activity (Miyashita et al., 2004). Expression of a Myc epitope-tagged form of NWASP–CRIB also prevented the effects of ectopic CD47 on the numbers of primary dendrites and branches from the longest primary dendrite, although it did not affect these parameters in neurons not overexpressing CD47 (Fig. 4*Ac*,*Af*,*B*,*C*). In addition, expression of NWASP–CRIB prevented the increase in the density of dendritic filopodia and spines apparent in neurons overexpressing CD47 and plated on SHPS-1–Fc (Fig. 4*D*).

We next determined whether forced expression of CD47 could promote the activation of Rac or Cdc42 in hippocampal neurons by the use of FRET imaging, which used the FRET probes Raichu–Rac and Raichu–Cdc42 (Itoh et al., 2002). The FRET imaging showed marked increases of the values of yellow fluorescent protein (YFP)/cyan fluorescent protein (CFP) ratio, with both Raichu–Rac and Raichu–Cdc42, at dendrites from CD47-expressing hippocampal neurons compared with that apparent with control mock-transfected neurons (Fig. 5*A*,*B*). These results suggest that forced expression of CD47 indeed induces activation of both Rac and Cdc42 in hippocampal neurons.